Atmos. Chem. Phys. Discuss., 15, 13109–13166, 2015
www.atmos-chem-phys-discuss.net/15/13109/2015/
doi:10.5194/acpd-15-13109-2015

Atmospheric Chemistry and Physics Discussions

Analysis of isothermal and cooling rate dependent immersion freezing by a unifying stochastic ice nucleation model

P. A. Alpert[1,*] **and D. A. Knopf**[1]

[1]Institute for Terrestrial and Planetary Atmospheres/School of Marine and Atmospheric Sciences, Stony Brook University, Stony Brook, NY 11794-5000, USA
[*]now at: Institut de Recherches sur la Catalyse et l'Environnement de Lyon, Centre National de la Recherche Scientifique, Université Claude Bernard Lyon 1, 69626 Villeurbanne, France

Received: 14 April 2015 – Accepted: 17 April 2015 – Published: 5 May 2015

Correspondence to: P. A. Alpert (peter.alpert@ircelyon.univ-lyon1.fr) and D. A. Knopf (daniel.knopf@stonybrook.edu)

Published by Copernicus Publications on behalf of the European Geosciences Union.

Abstract

Immersion freezing is an important ice nucleation pathway involved in the formation of cirrus and mixed-phase clouds. Laboratory immersion freezing experiments are necessary to determine the range in temperature (T) and relative humidity (RH) at which ice nucleation occurs and to quantify the associated nucleation kinetics. Typically, isothermal (applying a constant temperature) and cooling rate dependent immersion freezing experiments are conducted. In these experiments it is usually assumed that the droplets containing ice nuclei (IN) all have the same IN surface area (ISA), however the validity of this assumption or the impact it may have on analysis and interpretation of the experimental data is rarely questioned. A stochastic immersion freezing model based on first principles of statistics is presented, which accounts for variable ISA per droplet and uses physically observable parameters including the total number of droplets (N_{tot}) and the heterogeneous ice nucleation rate coefficient, $J_{het}(T)$. This model is applied to address if (i) a time and ISA dependent stochastic immersion freezing process can explain laboratory immersion freezing data for different experimental methods and (ii) the assumption that all droplets contain identical ISA is a valid conjecture with subsequent consequences for analysis and interpretation of immersion freezing.

The simple stochastic model can reproduce the observed time and surface area dependence in immersion freezing experiments for a variety of methods such as: droplets on a cold-stage exposed to air or surrounded by an oil matrix, wind and acoustically levitated droplets, droplets in a continuous flow diffusion chamber (CFDC), the Leipzig aerosol cloud interaction simulator (LACIS), and the aerosol interaction and dynamics in the atmosphere (AIDA) cloud chamber. Observed time dependent isothermal frozen fractions exhibiting non-exponential behavior with time can be readily explained by this model considering varying ISA. An apparent cooling rate dependence of J_{het} is explained by assuming identical ISA in each droplet. When accounting for ISA variability, the cooling rate dependence of ice nucleation kinetics vanishes as expected from classical nucleation theory. The model simulations allow for a quantitative exper-

ACPD
15, 13109–13166, 2015

imental uncertainty analysis for parameters N_{tot}, T, RH, and the ISA variability. In an idealized cloud parcel model applying variability in ISAs for each droplet, the model predicts enhanced immersion freezing temperatures and greater ice crystal production compared to a case when ISAs are uniform in each droplet. The implications of our results for experimental analysis and interpretation of the immersion freezing process are discussed.

1 Introduction

Ice crystals in tropospheric clouds form at altitudes where temperatures fall below the ice melting point, also known as supercooled temperatures, and for conditions in which water partial pressure exceeds the saturation vapor pressure with respect to ice (Pruppacher and Klett, 1997; Hegg and Baker, 2009). Cirrus or mixed-phase clouds consist entirely of ice crystals or of ice crystals coexisting with supercooled aqueous droplets, respectively. These clouds can significantly impact the global radiative budget and the hydrological cycle (Baker, 1997; Rossow and Schiffer, 1999; Chen et al., 2000; Liu et al., 2007; Lohmann and Hoose, 2009; Tao et al., 2012; Rosenfeld et al., 2014), however, their formation is not well understood or constrained in cloud and climate models (Boucher et al., 2013). Ice nucleation precedes the formation of ice crystals. Homogeneous ice nucleation occurs from supercooled aqueous aerosol particles or cloud droplets. Ice formation can also occur at temperatures higher than the homogeneous freezing limit initiated by insoluble particles acting as ice nuclei (IN). Heterogeneous ice nucleation can occur when IN are immersed in supercooled aqueous droplets, termed immersion freezing, when IN make physical contact with supercooled droplets, termed contact freezing, or when ice nucleates on IN directly from the supersaturated vapor phase, termed deposition ice nucleation. It is impossible to observe in situ ice nucleation in the atmosphere and very difficult to infer the ice nucleation pathway (Haag et al., 2003; Hegg and Baker, 2009). Despite the established importance of the impact

ACPD
15, 13109–13166, 2015

of heterogeneous ice nucleation on cirrus and mixed-phase cloud formation, it is not included in global radiative forcing estimates (Myhre et al., 2013).

Laboratory studies are necessary to investigate at which thermodynamic conditions, i.e. temperature, T, and relative humidity, RH, and by which mode ice nucleation occurs for predictive use in cloud and climate models. This study presents a newly developed model simulation applied for analyses of previously published laboratory immersion freezing data obtained by different experimental methodologies. It allows prediction of atmospheric ice particle production under relevant scales of time and IN surface area (ISA).

Classical Nucleation Theory (CNT) is currently the only available physical theory to describe ice nucleation. Simply stated, CNT quantifies a maximum Gibbs free energy barrier corresponding to the minimum number of water molecules in a cluster that has to be overcome to initiate ice nucleation (Pruppacher and Klett, 1997). Cluster formation and thus, ice nucleation, occurs stochastically and is dependent on time, t, and in the case of homogeneous ice nucleation, the supercooled liquid volume, V. Koop et al. (2000) parameterized the theoretical homogeneous ice nucleation rate coefficient, J_{hom}, as a function of T and water activity, a_{w} ($a_{\mathrm{w}} = 1.0$ for pure water and $a_{\mathrm{w}} < 1.0$ for aqueous solution). This approach yields J_{hom} to be independent of the nature of the solute and avoids the weakness of the capillary approximation in CNT (Pruppacher and Klett, 1997).

Immersion freezing can be described by CNT by reducing the free energy barrier due to the presence of a solid surface. Ice nucleation remains a stochastic process, but is dependent on the available ice nucleating surface area, A, instead of V (Pruppacher and Klett, 1997; Zobrist et al., 2007). The heterogeneous ice nucleation rate coefficient, J_{het}, is a physically and experimentally defined parameter which gives the rate of nucleation events for given surface area and unit time. By definition, J_{het} is a material specific parameter, similar to a second order rate constant in gas-phase kinetics. Knopf and Alpert (2013) parameterized J_{het} as a function of T and a_{w} following Koop et al. (2000) using direct measurements of J_{het} and J_{het} derived from previous

ACPD
15, 13109–13166, 2015

studies (Archuleta et al., 2005; Alpert et al., 2011a, b; Knopf and Forrester, 2011; Murray et al., 2011; Broadley et al., 2012; Iannone et al., 2011; Pinti et al., 2012; Rigg et al., 2013). Known as the a_w based immersion freezing model (ABIFM) (Knopf and Alpert, 2013), J_{het} can be derived for different types of IN such as mineral dusts, organic, surfactant and biogenic, applicable for $a_w \leq 1.0$, and independent of the nature of the solute. The ABIMF is a holistic and computationally efficient physical description of the immersion freezing process for prediction of ice nucleation for atmospherically relevant conditions and applicable for a variety of experimental methods, including the droplet-on-substrate approach (Zobrist et al., 2007; Knopf and Forrester, 2011; Alpert et al., 2011a, b; Iannone et al., 2011; Murray et al., 2011; Rigg et al., 2013; Broadley et al., 2012), oil-encased droplets (Murray et al., 2011; Broadley et al., 2012), differential scanning calorimetry (Pinti et al., 2012), and continuous flow diffusion chamber (Archuleta et al., 2005).

One major difficulty of many experimental techniques is the assessment of determining the accuracy and uncertainty of T, RH, t, and A, and how these uncertainties affect interpretation of laboratory ice nucleation experiments and corresponding ice nucleation parameterization and extrapolation to atmospherically relevant conditions (Connolly et al., 2009; Lüönd et al., 2010; Niedermeier et al., 2010; DeMott et al., 2010; Niedermeier et al., 2011; Hoose and Möhler, 2012; Niemand et al., 2012; Rigg et al., 2013; Hiranuma et al., 2015; Vali and Snider, 2015). This is especially important for non-physical (or empirical) parameterizations that are fitted to measured frozen fractions and ice crystal concentrations and thus, are inherently constrained to the investigated range of T, RH, t, A and concentration of IN (Rigg et al., 2013; Knopf and Alpert, 2013). These include the multi-component model (Murray et al., 2011), the time-dependent freezing rate parcel model (Vali and Snider, 2015), parameterizations of IN per liter of air (DeMott et al., 2010), the α-PDF model (Marcolli et al., 2007; Lüönd et al., 2010), the active site model (Marcolli et al., 2007; Lüönd et al., 2010), the singular description (Vali, 1971; Connolly et al., 2009; Alpert et al., 2011a, b; Vali, 2008; Murray et al., 2011; Hiranuma et al., 2015) and the soccer ball model (Niedermeier

ACPD
15, 13109–13166, 2015

et al., 2011), in which the latter 4 assume that ice preferentially occurs on ice active sites located on the particle surface. According to the singular hypothesis, the number of active sites, $n_s(T)$, is dependent on T only. Furthermore, these parameterizations cannot describe the freezing point depression (e.g. Zuberi et al., 2002; Archuleta et al., 2005; Koop and Zobrist, 2009) and nucleation kinetics (in analogy of homogeneous ice nucleation) observed in immersion freezing experiments where the IN are immersed in aqueous solution droplets (Rigg et al., 2013; Knopf and Alpert, 2013). These limitations clearly support further analytical efforts to improve our understanding on the governing parameters of immersion freezing.

The immersed ISA per droplet is important for experimental derivation of J_{het} and for deriving empirical quantities such as $n_s(T)$ or other fitting functions and their parameters. In previous experimental studies, droplets for ice nucleation experiments were dispensed from a bulk solution containing IN (Broadley et al., 2012; Rigg et al., 2013; Wright and Petters, 2013; Herbert et al., 2014; Diehl et al., 2014). In other investigations, solid particles were size selected by their electrical mobility and then injected into, or continuously flown through, an ice nucleation chamber where water condensation precedes ice nucleation (Archuleta et al., 2005; Kulkarni et al., 2012; Welti et al., 2012; Wex et al., 2014). In these studies and those that used polydisperse aerosol (e.g. Niemand et al., 2012), surface area calculations assumed that particles with the same mobility diameter are spherical with identical surface area. However, extensive theoretical and experimental literature exists on aerosol sizing instrumentation and morphology characterization, which consider particle density, void fraction, shape and electrical charge effects implying their non-sphericity (DeCarlo et al., 2004; Slowik et al., 2004; Zelenyuk et al., 2006; Schmid et al., 2007; Park et al., 2008). In general, neglecting these effects likely influences surface area estimates. Also, distributions of immersed ISA per droplet are typically assumed to be monodispersed, or in other words, each droplet is assumed to contain identical ISA. Furthermore, the number of droplets applied in an ice nucleation experiment may also affect the significance of the freezing data and thus interpretation of the experiment. It is necessary to question if a potential

ACPD
15, 13109–13166, 2015

variability in ISA and/or the assumption of monodisperse ISA and a limited number of observed freezing events become important for interpretation of immersion freezing experiments with subsequent ramifications for the analytical ice nucleation description.

We introduce a newly developed model simulation in which ice nucleation is treated explicitly as a stochastic process applicable for isothermal and cooling rate experiments. Previous experimental results using different experimental methods are simulated and compared for a wide range of atmospherically relevant conditions. Sensitivity studies on frozen fraction data and experimentally derived J_{het} are performed as a function of ISA assumptions, the number of droplets employed in the experiment, T, and RH. The validity of typical assumptions of ISA variability and uncertainty are tested. Then, a detailed analysis of the ability of the model simulation to reproduce experimental results with strict uncertainty estimation is presented for 7 independent immersion freezing studies utilizing 8 different instrumentation: (i) droplets on a cold-stage exposed to air, (ii) droplets on a cold-stage covered in oil, (iii) oil-droplet emulsions, (iv) droplet acoustic levitation, (v) droplet wind tunnel levitation, (vi) the Leipzig aerosol cloud interaction simulator (LACIS), (vii) a continuous-flow diffusion chamber (CFDC) and (viii) the aerosol interaction and dynamics in the atmosphere (AIDA) cloud chamber. A rigorous uncertainty analysis of the ice nucleation kinetics for typical ranges in experimental conditions is presented. The atmospheric implications by application of a simple cloud model are discussed.

2 Immersion freezing model based on classical nucleation theory

2.1 Simulation of isothermal freezing experiments

Stochastic immersion freezing simulations (IFSs) are performed to evaluate the effect of variable ISA on droplet immersion freezing experiments conducted in the laboratory. As discussed above, different droplets in a laboratory experiment will possess different ISA. To account for this fact, ISA in each simulated droplet is sampled from a lognormal

ACPD
15, 13109–13166, 2015

distribution to mimic this variability with the most probable ISA being A_g or a mean distribution parameter $\mu = \ln(A_g)$. The distribution width parameter is $\sigma = \ln(\sigma_g)$, where σ_g represents the factor by which ISA can vary. Knowledge of ISA for each droplet can be directly used as an alternative without a need for random sampling. Droplet freezing for isothermal experiments can then be described by

$$\delta N_{ufz} = -J_{het} A_{tot} \delta t, \quad (1)$$

where δN_{ufz} represents the change in the number of unfrozen droplets after a certain interval of time, δt, and J_{het} is the heterogeneous ice nucleation rate coefficient. The total available ISA is $A_{tot} = \sum A_j$, where A_j is the ISA in the jth droplet. Equation (1) is typically simplified by assuming all droplets contain the same ISA (e.g. Marcolli et al., 2007; Lüönd et al., 2010; Niedermeier et al., 2010; Murray et al., 2011; Rigg et al., 2013). However, when taking into account individual droplet ISA, this assumption is not valid. Since the ISA variability cannot be resolved from experiments, a droplet freezing simulation must be employed to model ice nucleation for interpretation purposes. To accomplish this, freezing of each single droplet is assumed to be stochastic, or in other words, there exists a probability of the jth droplet to freeze, $P_{j,frz}$, within δt. The probability for a single droplet not to freeze, $P_{j,ufz}$, is realized as an exponential decay law (Pruppacher and Klett, 1997; Koop et al., 1997) and therefore,

$$P_{j,frz} = 1 - P_{j,ufz} = 1 - e^{-J_{het} A_j \delta t}. \quad (2)$$

We apply a time and surface area dependent immersion freezing process which follows CNT and therefore, all simulations employ J_{het} having units of $cm^{-2}\,s^{-1}$. However, J_{het} does not explicitly depend on time and ISA, but on T and a_w. A droplet can either remain in an unfrozen state or freeze and therefore, is described exactly by a binomial distribution, $B(k; n, P_{j,frz})$, with parameters $P_{j,frz}$ given by Eq. (2) and $n = 1$ meaning that only one trial is given for an individual droplet to freeze in δt. A randomly sampled number, $k = 0$ or 1, is obtained from the distribution

$$B(k; n = 1, P_{j,frz}) = P_{j,frz}^{k} (1 - P_{j,frz})^{1-k} \quad (3)$$

ACPD
15, 13109–13166, 2015

for each droplet with a normalization prefactor, $n!/(k!(n-k)!) = 1$. When $k = 1$, freezing occurs for the jth droplet and if $k = 0$, the droplet does not freeze and another k is sampled in the next time interval. For a collection of multiple droplets, the number of freezing events that occur in a given time interval is n_{frz} and the cumulative sum as a function of time is $N_{frz}(t)$. For a single IFS starting with N_{tot} liquid droplets, the fraction of unfrozen droplets is $f_{ufz}(t) = 1 - N_{frz}(t)/N_{tot}$.

A record of n_{frz} and corresponding droplet ISA, i.e. A_j, is kept for a single IFS. This record can be thought of as a simulated experimental immersion freezing data set, i.e. it gives a record of droplet freezing time while tracking A_j. Due to the stochastic nature of nucleation, repetition of isothermal IFSs will not result in identical values of f_{ufz} over t. Likewise, repetition of a laboratory experiment will not result in exactly the same $f_{ufz}(t)$ curve. Therefore it is necessary to repeat the simulations in order to reveal a range of $f_{ufz}(t)$ values of which the mean unfrozen fraction, $\bar{f}_{ufz}(t)$, can be derived from all simulations. We choose an ensemble of 10^5 IFSs to accurately determine $\bar{f}_{ufz}(t)$. This procedure is a basic form of a Monte Carlo method and yields upper and lower percentile bounds at 5 and 95 % serving as a statistical uncertainty of the immersion freezing process.

An ensemble of IFSs, referred to as a model simulation, requires the selection of parameters N_{tot}, A_g, σ_g, and J_{het}. For demonstration purposes, the parameter choice is arbitrary. However, when reproducing a laboratory derived data set, a parameter selection process is applied. Parameters which can be directly accessed from previous laboratory studies are first selected to mimic experimental conditions. For example, if a study reports that 100 droplets were used in an immersion freezing experiment, then $N_{tot} = 100$, or if the average ISA is reported as $7.1 \times 10^{-6}\,cm^2$, then $A_g = 7.1 \times 10^{-6}\,cm^2$. For all studies in which a parameter is not available or easily calculated, an estimate which best reproduces experimental conditions is determined. In many isothermal immersion freezing laboratory studies, droplet freezing continues over time when all other conditions remain constant, i.e. at constant T (Wright and Petters, 2013;

ACPD
15, 13109–13166, 2015

Murray et al., 2011; Broadley et al., 2012; Herbert et al., 2014). Therefore, the J_{het} parameter is selected to be constant for isothermal IFSs.

2.2 Simulation of cooling rate dependent immersion freezing experiments

2.2.1 Experimentally derived J_{het} for model input

When a cooling rate is applied in model simulations, droplet freezing is simulated in discrete temperature intervals and therefore J_{het} at every step is required for deriving $P_{j,frz}$. In this study, only water droplets are considered and therefore, it is assumed that $a_w = 1.0$ and J_{het} becomes a function of T only. Ideally, experimentally derived $J_{het}(T)$ should be used for prediction of immersion freezing. However, these data sets are usually limited in T range and are discrete in nature. Knopf and Alpert (2013) compiled and parameterized experimental J_{het} data yielding a continuous function over T called the ABIFM and expressed as,

$$\log_{10}(J_{het}) = m\Delta a_w + c, \quad (4)$$

where m and c are slope and intercept parameters, respectively, and Δa_w is the independent variable following the formulation of Koop et al. (2000). The Δa_w at which a droplet freezes is calculated by subtracting the a_w of the droplet (= 1.0 for pure water) from the water activity point that falls on the ice melting curve, $a_{w,\,ice}(T)$, at the same temperature or

$$\Delta a_w = a_w(T) - a_{w,\,ice}(T), \quad (5)$$

where

$$a_{w,\,ice}(T) = p_{ice}(T)/p^{\circ}{}_{H_2O}(T), \quad (6)$$

and $p_{ice}(T)$ and $p^{\circ}{}_{H_2O}$ are the vapour pressure with respect to planar ice and water, respectively (Murphy and Koop, 2005).

ACPD
15, 13109–13166, 2015

Resulting calculations from Eqs. (4) to (6) are not computationally demanding and conveniently derive $J_{het}(T)$ for model input. Note that for isothermal model simulations, a continuous function of J_{het} is not required and thus model derived J_{het} is independent from the ABIFM.

2.2.2 Simulated droplet freezing

Cooling rate dependent IFSs are performed to evaluate the effect of stochastic freezing and variable ISA in laboratory immersion freezing experiments. Again, the ISA for a single droplet is sampled from a lognormal distribution, however, Eqs. (1) and (2) are modified to

$$\delta N_{ufz} = -\frac{A_{tot}}{r} J_{het}(T)\delta T, \tag{7}$$

and

$$P_{j,frz} = 1 - P_{j,ufz} = 1 - e^{-\frac{A_j}{r} J_{het}(T)\delta T}, \tag{8}$$

respectively, where δT is a temperature interval and $r = \delta T/\delta t$ is the cooling rate. $J_{het}(T)$ is calculated from Eq. (4) and used in Eq. (8). Once the probability for the jth droplet to freeze is calculated for all droplets, freezing is determined by sampling from $B(k; n, P_{j,frz})$ (Eq. 3). The number of freezing events that occur in a given δT is n_{frz}, and the cumulative sum as a function of T is $N_{frz}(T)$ and used to calculate frozen fractions of droplets, $f_{frz}(T) = N_{frz}(T)/N_{tot}$. Similar to isothermal freezing, a single r dependent IFS yields a droplet immersion freezing record analogous to an experimental data set. In this case, the record of droplet freezing and corresponding A_j is a function of T. The average frozen fraction for 10^5 simulations, $\bar{f}_{frz}(T)$, is calculated along with percentiles at 5 and 95 %, the latter used as a statistical uncertainty.

It is important to note that application of r dependent IFSs presented here do not require the ABIFM, as it is only used as a parameterization of previously published

ACPD
15, 13109–13166, 2015

immersion freezing data sets to calculate $J_{het}(T)$. Any other published $J_{het}(T)$ will work equally as well. The ABIFM parameterization is IN type dependent and suitable for saturated and subsaturated conditions, i.e. $a_w \leq 1$, or RH $\leq 100\,\%$, if the droplet is in equilibrium with the water vapor phase. Aqueous solution droplets containing IN and having $a_w < 1.0$ will decrease J_{het} for the same T when compared with pure water droplets, an effect captured by ABIFM (Knopf and Alpert, 2013). Therefore, the ABIFM is a useful and convenient tool for model input $J_{het}(T)$.

3 Results and discussion

3.1 Isothermal model simulations of individual droplet freezing experiments

Figure 1a shows 5 and 95 % bounds of f_{ufz} from 4 model simulations for different N_{tot} applying either uniformly equal ($\sigma_g = 1$) or lognormally distributed ($\sigma_g = 10$) ISA per droplet as given in Table 1. For Iso1 and Iso2 having uniform ISA, f_{ufz} (on a logarithmic scale) is linear with t. However, the spread of the 5 and 95 % bounds is much wider for Iso2 having $N_{tot} = 30$ than for Iso1 having $N_{tot} = 1000$. It is clear that a larger spread in simulated f_{ufz} is entirely due to applied smaller N_{tot}. This implies that a laboratory experiment using a small N_{tot}, is statistically less significant compared to an experiment with greater N_{tot}. A single experimentally derived f_{ufz} curve under the same conditions as Iso2 will fall anywhere between the upper and lower bounds, and thus may even appear to deviate from a log-linear relationship over time. Therefore, interpretation about the nature of the heterogeneous ice nucleation process from the slope of f_{ufz} over time for an experiment using small N_{tot} should be conducted with care.

Model simulations Iso3 and Iso4 are shown in Fig. 1a where $N_{tot} = 1000$ and 30, respectively, and the ISA per droplet is sampled from lognormal distribution with $\sigma_g = 10$. In Iso3, f_{ufz} significantly deviates from a log-linear relationship with t. In Iso4, the same curvature exists, however the percentile bounds are much wider due to applied smaller N_{tot}. It is important to note that J_{het} is the same and constant for all simulations shown

ACPD
15, 13109–13166, 2015

in Fig. 1a. The nucleation rate of each jth droplet can be calculated as, $\omega_{het,j} = J_{het} A_j$ with units of s^{-1}. The droplets having a larger or smaller ISA will result in larger or smaller $\omega_{het,j}$, respectively. The fact that f_{ufz} is linear for $\sigma_g = 1$, the curvature effect in f_{ufz} seen for $\sigma_g = 10$ must be entirely due to ISA variability. This is because droplets with greater values of $\omega_{het,j}$ will tend to nucleate more rapidly than those having smaller $\omega_{het,j}$ values. In other words, the curvature of $f_{ufz}(t)$ is entirely due to those droplets having larger and smaller ISA that freeze within shorter and longer time scales, respectively. In addition, the spread in the 5 and 95 percentiles is very similar for Iso1 and Iso3, and for Iso2 and Iso4. This is seen most clearly at the intersection of the blue and green shaded regions ($t \simeq 1.3$ min). This implies that in isothermal freezing experiments, variability in ISA will not significantly affect stochastic uncertainty estimates, but will cause $f_{ufz}(t)$ to deviate from a log-linear relationship. From this we can conclude that the effects of droplet numbers and ISA variability on f_{ufz} can be decoupled and independently assessed. Consequentially, any interpretation on the physical process of immersion freezing based on the slope of f_{ufz} is unfounded.

In some previous experimental isothermal immersion freezing studies, the number of liquid droplets and an estimate of the average ISA per droplet are provided or can be derived. However, the validity of the assumption that all droplets possess the same ISA is rarely investigated or quantified. Similarly, J_{het} is not often reported. However, laboratory data do provide an opportunity to test our model for robustness while using parameters similar to those reported in the experimental studies. In fact, our model can also provide estimates for parameters typically unreported or unavailable, such as J_{het} and σ_g.

Experimental data by Wright and Petters (2013) for isothermal immersion freezing by Arizona Test Dust (ATD) is very well reproduced by model simulation IsoWR as demonstrated in Fig. 1b. Parameters for IsoWR are given in Table 1 and chosen to mimic experimental conditions in which droplets contained 1 wt% ATD held at 251 K. Bounds at 5 and 95 % of simulated f_{ufz} are shown in Fig. 1b and envelop the laboratory data. A repeat experiment by Wright and Petters (2013) should result in a f_{ufz} curve

ACPD
15, 13109–13166, 2015

falling within the percentile bounds 95 % of the time when considering only stochastic uncertainty.

To further evaluate the validity of the simulations, the parameters used are compared with experimental conditions given in Wright and Petters (2013). IsoWR uses $N_{tot} = 1000$ which agrees with the reported range of 300–1500. The next parameter in question is $\sigma_g = 9.5$, which can be interpreted as a systematic standard error in ISA due to the experimental methods of generating or dispensing droplets containing ATD acting as IN. We note this is different from an absolute ISA measurement error. Wright and Petters (2013) emulsified a mixture of oil and a bulk solution of water and ATD particles to form droplets with diameters of 50–250 µm. The variability in ISA should scale directly with the variability in droplet volumes (over 2 orders of magnitude), the variability in ATD particle numbers, and the variability in ATD particle size. While not directly defined by Wright and Petters (2013), we are confident that the overall range in ISA should be well over 2 orders of magnitude and therefore, $\sigma_g = 9.5$ is a reasonable value for the lognormal distribution width parameter employed in the simulations in Fig. 1b to reproduce the experimental data. The third parameter in question is $A_g = 6.4 \times 10^{-3}\,cm^2$. Unfortunately, an average ISA was not reported by Wright and Petters (2013), but can be estimated using literature values of specific surface area (SSA) applying the Brunauer, Emmett and Teller gas adsorption method (Brunauer et al., 1938). Bedjanian et al. (2013) report SSA for ATD used in Wright and Petters (2013) as $85 \pm 10\,m^2\,g^{-1}$. The ISA per drop can then be estimated from the drop volume, V_{drop}, and the density of water, ρ_w, using the equation $V_{drop} \cdot \rho_w \cdot wt\,\% \cdot SSA$. Considering only the variability in V_{drop}, average ISA per drop should range between 5.5×10^{-4} and $7.0 \times 10^{-2}\,cm^2$. The A_g parameter in model simulation IsoWR falls within this range. Finally, J_{het} for ATD in water droplets was investigated by Pinti et al. (2012) who reanalyzed ATD immersion freezing data by Marcolli et al. (2007) but did not report J_{het} values. However, estimates can be made following Knopf and Alpert (2013) accounting for $f_{frz} = 0.01$ and a nucleation time assumed to be 1 s, which yields J_{het} ranging from

ACPD
15, 13109–13166, 2015

5×10^6 to $1 \times 10^2\,\mathrm{cm^{-2}\,s^{-1}}$ between $T = 247.4$ and 252.8 K, in reasonable agreement with $J_{het} = 2.6 \times 10^3\,\mathrm{cm^{-2}\,s^{-1}}$ used in IsoWR at 251 K.

The new model simulation presented here based entirely on CNT can describe freezing experiments by Wright and Petters (2013) accounting for long nucleation time scales and a large number of droplets considering variability in ISA. In addition, all crucial parameters applied are experimentally supported, in particular J_{het} which is in agreement with independent studies (Marcolli et al., 2007; Pinti et al., 2012). Therefore, the isothermal immersion freezing data set of Wright and Petters (2013) can be entirely explained by a time and ISA dependent stochastic freezing process, in which each droplet contains variable ISA.

Figure 2 shows results of isothermal freezing experiments by Broadley et al. (2012) for illite compared to model simulation IsoBr and experimental results by Herbert et al. (2014) for the IN types kaolinite and feldspar compared to model simulations IsoHE1 and IsoHE2, respectively (see Table 1). The experimental data and $\bar{f}_{ufz}$ for all model simulations are in agreement and fall within the percentile bounds. Notice that the scatter in the isothermal immersion freezing data points is much larger than for Wright and Petters (2013) shown in Fig. 1b. As previously discussed, this is entirely due to a smaller number of droplets used in the laboratory experiments by Broadley et al. (2012) ($N_{tot} = 63$) and Herbert et al. (2014) ($N_{tot} = 40$) and thus, can be entirely attributed to the stochastic nature of immersion freezing as expected by CNT. The model simulations capture this effect by producing a wide range in f_{ufz}. Only one experiment was performed for each of the laboratory data sets presented in Fig. 2 and if these experiments were repeated, f_{ufz} values would very likely not be the same and may even exhibit a more linear or curved behavior with time. Repetition of experiments should provide better estimates of $\bar{f}_{ufz}$ and σ_g, but for any single experiment, f_{ufz} would still fall within the given percentile bounds. In other words, additional experiments would better define the mean of f_{ufz} and the uncertainty in the mean of f_{ufz}, but will not decrease the uncertainty bounds. Only by using more droplets, e.g. Wright and Petters (2013), would a single experiment be more statistically significant.

ACPD
15, 13109–13166, 2015

Parameters A_g and N_{tot} used in IsoBR are directly provided and used (Broadley et al., 2012). Droplet volumes in the experiment by Broadley et al. (2012) (Fig. 2a) varied by an order of magnitude. Considering the additional variability in particle numbers and size, total ISA variability should be larger than 1 order of magnitude. For IsoBR, σ_g = 8.3, in agreement with experimental conditions. J_{het} derived at T = 243.3 K by ABIFM is $1.25 \times 10^3\,cm^{-2}\,s^{-1}$ and is in excellent agreement with model derived J_{het} at the same experimentally investigated T. Thus, laboratory derived isothermal immersion freezing of illite is entirely explained by CNT accounting for the stochastic nature of immersion freezing and variability in ISA.

The model simulation IsoHe1 shown in Fig. 2b uses the parameter $A_g = 1.2\,cm^2$, in good agreement with experimentally derived $A_g = 2.4\,cm^2$, for kaolinite using SSA = $11.8\,m^2\,g^{-1}$ (Murray et al., 2011), 1.0 wt % concentration and V_{drop} = 1 µL. Herbert et al. (2014) did not report sufficient information to estimate an overall variability in ISA, therefore, comparison of σ_g to experimental conditions is difficult. As previously discussed, repetition of experiments would result in f_{ufz} exhibiting possibly more linear or non-linear behavior with t within the calculated percentile bounds, which results in smaller or larger values of σ_g, respectively. Herbert et al. (2014) assumed that each droplet possessed the same ISA, however, this assumption is not supported due to the large statistical uncertainty from the small number of applied droplets. In order to better assess σ_g, more experiments or employing a larger number of droplets are needed to obtain more accurate $\bar{f}_{ufz}$ values. The ABIFM yields $J_{het} = 1.75 \times 10^{-2}\,cm^{-2}\,s^{-1}$ at T = 255.15 K and a_w = 1.0 which is within an order of magnitude of J_{het} used in IsoHE1. The agreement between simulated and experimental parameters implies that CNT can explain observed immersion freezing of kaolinite when variable ISA and stochastic uncertainty is considered.

Immersion freezing data of Herbert et al. (2014) for feldspar is reproduced by the model simulation IsoHE2. The parameters for IsoHE2 are given in Table 1. Average ISA for the data in Fig. 2 is $1.85 \times 10^{-2}\,cm^2$, similar to $A_g = 2.0 \times 10^{-2}\,cm^2$ used in

ACPD
15, 13109–13166, 2015

IsoHE1. Droplets used in Herbert et al. (2014) were dispensed with a digital micropipet with high accuracy, thus it can be expected that the contribution of droplet volume variability to the σ_g parameter is low. However, large uncertainty in f_{ufz} limits a reliable experimental estimate of σ_g for comparison with model derived σ_g. To better constrain σ_g, more statistical certainty is required by application of more droplets or conducting multiple experiments. Values of J_{het} for feldspar independent from Herbert et al. (2014) to our knowledge do not exist making comparison difficult.

Model simulations IsoDI1-3 of isothermal immersion freezing experiments by Diehl et al. (2014) for illite acting as IN in wind tunnel levitation experiments are shown in Fig. 3. Simulation parameters are given in Table 1. Only one droplet was observed in each experiment, and approximately 45 experiments were conducted for each of the 3 data sets shown in Fig. 3. This is equivalent to 1 experiment with $N_{tot} = 45$ droplets, since droplet freezing is independent of the freezing of other droplets. Excellent agreement is observed between simulated and experimental f_{ufz}. At $T = -18$ and $-21\,^{\circ}\mathrm{C}$, the ABIFM yields $J_{het} = 1.8 \times 10^{-2}$ and $2.6 \times 10^{-1}\,\mathrm{cm}^{-2}\,\mathrm{s}^{-1}$, respectively, and is in excellent agreement with derived values in IsoDI1-3. It can be expected that σ_g is the same for all three simulations, due to the fact that Diehl et al. (2014) likely used identical bulk water-illite solution stock. However, the large uncertainties do not allow for an adequate constraint of σ_g. Nevertheless, we can still conclude that immersion freezing is a time dependent stochastic process reconciled only when variable ISA is considered.

Depending on ISA variability, trajectories of model derived f_{ufz} over time are significantly altered and thus assuming identical ISA is not valid. It is well known that immersion freezing depends on surface area, i.e. an increase in ISA translates to an increase in nucleation rate for time. However, we note that variability in both t and ISA equally affect calculations of droplet freezing probabilities (Eq. 2) used in model simulations, and therefore neglecting time dependence will cause erroneous interpretation of immersion freezing data to the same degree as if the surface area dependence is neglected. This simple stochastic immersion freezing model accounting for ISA variability can explain the isothermal ice nucleation data of various experiments without invoking

ACPD
15, 13109–13166, 2015

empirical parameterizations, assumptions of particle surface composition, and/or other modifications in parameters and interpretations.

3.2 Cooling rate model simulations of individual droplet freezing experiments

Cooling rate IFSs were performed to investigate the effects of variable ISA and N_{tot} on experimentally derived J_{het} and f_{frz} as a function of T. For a single cooling rate IFS, variable ISA per droplet is applied and used to calculate $P_{j,frz}$ from Eq. (8), and then Eq. (3) simulates freezing. Discrete δT steps are used in cooling IFSs and thus, this process is repeated for all droplets which remained unfrozen at each consecutive δT. The IFS stops after some T or when all droplets freeze, and the simulated freezing record is kept detailing which droplets froze or remained liquid at each T and their corresponding ISA. This is analogous to running an immersion freezing experiment in a laboratory setting and recording the observed number of frozen droplets or ice crystals as a function of T.

The simulated freezing record is treated as a freezing data set from which the assumption of identical ISA can be tested. This is accomplished by re-calculating J_{het} from the simulated data. These (re-)calculations use n_{frz}, the length of the time interval, $\delta t = \delta T/r$, and either of two different approaches in determining A_{tot}. For the first approach, A_g is assumed to be identical for all droplets, i.e. without the knowledge that immersion freezing was simulated for droplets with variable ISA in the first place. This is equal to assuming a monodisperse IN population in laboratory immersion freezing experiments resulting in an "apparent" heterogeneous ice nucleation rate coefficient, $J_{het}^{apparent}(T)$, calculated by

$$J_{het}^{apparent}(T) = \frac{n_{frz}(T)}{n_{ufz}(T) A_g \frac{\delta T}{r}}, \quad (9)$$

where $n_{ufz}(T)$ is the number of unfrozen droplets at T and $A_{tot} = n_{ufz} A_g$. The second approach accounts for the variable ISA present in droplets resulting in the "actual"

ACPD
15, 13109–13166, 2015

heterogeneous ice nucleation rate coefficient, $J_{het}^{actual}(T)$, calculated by

$$J_{het}^{actual}(T) = \frac{n_{frz}(T)}{\sum A_j \frac{\delta T}{r}}, \quad (10)$$

and $A_{tot} = \sum A_j$ is the total surface area contribution from droplets that remain liquid. Comparing results from Eqs. (9) and (10) allows evaluation of the assumption that all droplets have the same ISA, when they actually do not. In this way a null hypothesis is considered, that is if $J_{het}^{apparent}(T)$ and $J_{het}^{actual}(T)$ are the same, then the assumption of identical ISA is valid.

Poisson statistics are used to derive upper and lower fiducial limits of $J_{het}^{apparent}(T)$ and $J_{het}^{actual}(T)$ at $x = 0.999$ confidence for n_{frz} following Koop et al. (1997). The upper fiducial limit of the heterogeneous ice nucleation rate coefficient, J_{het}^{up}, accounts for additional freezing events occurring with a probability of x, than observed n_{frz}. Likewise, a lower fiducial limit of the heterogeneous ice nucleation rate coefficient, J_{het}^{low}, accounts for less than the observed n_{frz} occurring with a probability of x. We refer to the upper and lower limits of n_{frz} as n_{frz}^{up} and n_{frz}^{low}, respectively (Koop et al., 1997). The fiducial limits of $J_{het}^{apparent}$ and J_{het}^{actual} for a single simulation can be calculated using Eqs. (9) and (10), but replacing n_{frz} with n_{frz}^{up} or n_{frz}^{low}, respectively. Each simulation results in different $J_{het}^{apparent}$ and J_{het}^{actual} values and different fiducial limits at the same T due to random sampling, therefore, averages are reported.

Figure 4 shows the results of two model simulations, Cr1 and Cr2, having $r = 0.5$ and $5.0\,K\,min^{-1}$, respectively. For all 10^5 IFSs, $\overline{J}_{het}^{apparent}$ and $\overline{J}_{het}^{actual}$ are shown in Fig. 4a and b as dashed lines, respectively, along with corresponding f_{frz} curves displayed in Fig. 4c and d. The parameterization of $J_{het}(T)$ for illite dust (Knopf and Alpert, 2013) with $m = 54.5$ and $c = -10.7$ used in Eq. (8) for each simulation is shown as the red line in Fig. 4a and b and referred to as the model input J_{het}. Simulation parameters for Cr1 and Cr2 are given in Table 2.

ACPD
15, 13109–13166, 2015

According to CNT, two immersion freezing cooling rate experiments conducted at different r should result in identical J_{het} values due to the fact that J_{het} is independent of r. CNT is violated if significantly different J_{het} values are derived at different r. Figure 4a shows that values of $\overline{J}_{het}^{apparent}$ are not the same for model simulations Cr1 and Cr2. Also $\overline{J}_{het}^{apparent}$ is overestimated at higher freezing temperatures and underestimated at lower freezing temperatures compared with model input $J_{het}(T)$. These significant differences do not support the null hypothesis and imply that when experimentally deriving J_{het}, the assumption that ISA per droplet is identical is invalid. Figure 4b shows that accounting for variable ISA, $\overline{J}_{het}^{actual}$ for Cr1 and Cr2 is consistent and in very good agreement with model input J_{het} (red curve) within the upper and lower fiducial limits. In addition, $\overline{J}_{het}^{actual}$ for the two simulations Cr1 and Cr2 are identical at the same T. We conclude that when accounting for variable ISA, immersion freezing results applying different r and ISA are consistent as predicted by CNT.

Towards warmer ($T > 248$ K) and colder temperatures ($T < 238$ K), the difference in upper and lower fiducial limits derived in Cr1 and Cr2 are much greater than for the mid temperature range ($238 < T < 248$ K). In fact the smallest difference occurs at $\overline{f}_{frz} \simeq 0.5$. This is because calculations are statistically more significant at the median freezing where n_{frz} is largest. Fewer droplets freeze at the beginning and end of a cooling process resulting in a wide fiducial limit range reaching up to 4 orders of magnitude (Fig. 4a and b) in spite of a high number of dropets used ($N_{tot} = 1000$). The corresponding percentile bounds of f_{frz} shown in Fig. 4c and d do not reflect a considerable uncertainty compared to the upper and lower fiducial limits (Fig. 4a and b). It is important to note that f_{frz} are identical in Fig. 4c and d, because surface area is not used to derive f_{frz}. This analysis suggest that values and uncertainties of f_{frz} are not suited to derive J_{het} and any corresponding error.

Previous immersion freezing experiments by Herbert et al. (2014) are modeled in CrHE1 and CrHE2 where $r = 0.2$ and $2.0\,\mathrm{K\,min^{-1}}$, respectively, for the case of feldspar acting as IN. The parameters σ_g and A_g from the IsoHE2 simulation are used in CrHE1

ACPD
15, 13109–13166, 2015

and CrHE2. Since Herbert et al. (2014) assumed identical ISA, experimentally derived J_{het} can be directly compared with $J_{het}^{apparent}$ from cooling rate model simulations.

Figure 5 shows experimentally derived f_{frz} and $J_{het}^{apparent}$ from Herbert et al. (2014) compared to results of model simulations CrHE1 and CrHE2. Parameters $m = 122.83$ and $c = -12.98$ are used in Eq. (4) to reproduce frozen fraction data (Fig. 5a) within 5 and 95 % bounds. The laboratory data falls within percentiles and fiducial limits of f_{frz} and $J_{het}^{apparent}$, respectively. The model simulations are robust since the same A_g and σ_g are used in both cooling rate and isothermal experiments. Figure 5b displays the good agreement between $J_{het}^{apparent}$, and experimental data. However, it also demonstrates that assuming uniform ISA causes an erroneous dependency of experimentally derived J_{het} on r. Figure 5c shows $\overline{J}_{het}^{actual}$ with upper and lower fiducial limits derived from CrHE1 and CrHE2. When accounting for variable ISA, $\overline{J}_{het}^{actual}$ are in excellent agreement with the ABIFM parameterization derived in this study for feldspar IN. Furthermore, $\overline{J}_{het}^{actual}$ calculated for different r are identical as predicted by CNT, a similar finding as in the model simulations Cr1 and Cr2 (Fig. 4b). Therefore, $J_{het}(T)$ used here can be considered a new $J_{het}(\Delta a_w)$ parameterization for feldspar.

The differences between $\overline{J}_{het}^{apparent}$ and $\overline{J}_{het}^{actual}$ shown in Figs. 4a, b and 5b, c are further discussed. After simulated freezing of droplets with variable ISA is complete, $J_{het}^{apparent}$ is calculated using the simulated droplet freezing record but, with the assumption that ISA is identical for all droplets equal to A_g. As previously discussed, this is analogous to observing droplet freezing in the laboratory and calculating J_{het} once the experiment is finished assuming identical ISA. The slope of $\overline{J}_{het}^{apparent}$ is less steep than for $\overline{J}_{het}^{actual}$ as a function of T. We note that surface area is inversely proportional to J_{het}. In the temperature range in which freezing is simulated, droplets with ISA less than A_g will likely freeze at colder T compared to droplets with ISA greater than A_g, which will likely freeze at warmer T. However, assuming identical ISA equal to A_g for all droplets

ACPD
15, 13109–13166, 2015

either overestimates or underestimates the actual ISA present in droplets that freeze at colder and warmer temperatures, respectively. Due to the inverse relationship between A_g and J_{het}, calculations of $\overline{J}_{het}^{apparent}$ from Eq. (9) will be underestimated and overestimated at colder and warmer temperatures, respectively. As a consequence, the slope of $\overline{J}_{het}^{apparent}$ is less steep compared to model input J_{het} (red curve) as demonstrated in Figs. 4a and 5b. Therefore, assuming identical ISA in each droplet not only results in erroneous J_{het} values (for various applied r), but also misrepresentation of the slope J_{het} vs. T. Furthermore, simulated and experimentally derived $J_{het}^{apparent}$ for $r = 0.2$ and $2.0\,K\,min^{-1}$ (Fig. 5b) are different by about 1 order of magnitude at the same T. In separate model simulations not shown here, applying r different by 2 orders of magnitude yields $J_{het}^{apparent}$ values that differ by 2 orders of magnitude. This means that assuming identical ISA in each droplet implicitly imposes a cooling rate dependence on $J_{het}^{apparent}$.

Model simulations CrDI1 and CrDI2 of immersion freezing experiments by Diehl et al. (2014) for illite acting as IN probed in acoustic levitation experiments are shown in Fig. 6. Simulation parameters are given in Table 2. A non-linear r was used in Diehl et al. (2014) and was the same for both experiments and model simulations, but the ISA per droplet was varied. Diehl et al. (2014) reported an ISA per drop of 7.1×10^{-1} and $7.1 \times 10^{-3}\,cm^2$ in the 2 different sets of experiments. When using these exact values in conjunction with the other parameters, model simulations cannot reproduce experimental f_{frz}. This is in spite of the excellent performance of IsoBr for reproducing droplet freezing initiated by illite IN from Broadley et al. (2012). In attempt to reconcile results from Diehl et al. (2014) with previous literature data (Broadley et al., 2012; Knopf and Alpert, 2013), model derived f_{frz} are fit to experimental f_{frz} yielding two different parameter values of $A_g = 2.94$ and $2.91 \times 10^{-2}\,cm^2$ used in CrDI1 and CrDI2, respectively. We note that fitted A_g values differ only by a factor of 4 from values reported by (Diehl et al., 2014) and therefore, are in reasonable agreement. However, calculated $J_{het}^{apparent}$

ACPD
15, 13109–13166, 2015

values shown in Fig. 6b still use ISA of 7.1×10^{-1} and $7.1 \times 10^{-3}\,\mathrm{cm}^2$ as reported by Diehl et al. (2014).

Figure 6a shows that simulated and experimental f_{frz} are in agreement when accounting for ISA variability ($\sigma_{\mathrm{g}} = 5.7$). Experimental values of $J_{\mathrm{het}}^{\mathrm{apparent}}$ displayed in Fig. 6b are in agreement with model derived $\overline{J}_{\mathrm{het}}^{\mathrm{apparent}}$. This result is robust since experimental $J_{\mathrm{het}}^{\mathrm{apparent}}$ data was not used in fitting f_{frz}. Accounting for the actual variability in ISA used to simulate freezing, $J_{\mathrm{het}}^{\mathrm{actual}}$ shown in Fig. 6c is in perfect agreement with the ABIFM parameterization for illite (Knopf and Alpert, 2013). Again, the data and model supports a stochastic, time dependent immersion freezing process to describe laboratory data considering variable ISA.

A major inconsistency in experimental and simulated $J_{\mathrm{het}}^{\mathrm{apparent}}$ shown in Fig. 6b is discussed for the case when different ISA are applied. According to CNT, J_{het} is independent of surface area. This means that if two experiments are performed with different ISA but use the same r, J_{het} should be the same as a function of T. However, simulated and experimentally derived $\overline{J}_{\mathrm{het}}^{\mathrm{apparent}}(T)$ deviate by more than 1 order of magnitude. Clearly, $J_{\mathrm{het}}^{\mathrm{apparent}}$ values violate CNT, but this is the cause of assuming identical ISA. In fact, this freezing behavior also contradicts all surface-based empirical parameterization of immersion freezing, such as determining $n_{\mathrm{s}}(T)$, or the number of actives sites per particle surface area (Murray et al., 2012; Hoose and Möhler, 2012). This result impacts all immersion freezing experiments conducted as a function of ISA that assume identical ISA, thereby implicitly imposing a surface area dependence on $J_{\mathrm{het}}^{\mathrm{apparent}}$ or $n_{\mathrm{s}}(T)$. However, accounting for the experimental uncertainty and variability in ISA reconciles experimental data.

3.3 Continuous flow and cloud chamber immersion freezing experiments

Model simulations IsoCFDC and IsoLACIS (see Table 1) reproduce experimental results of Wex et al. (2014) who used 2 ice nucleation instrumentation, (i) a continuous

ACPD
15, 13109–13166, 2015

flow diffusion chamber (CFDC) (Rogers et al., 2001; DeMott et al., 2010) and (ii) the Leipzig aerosol cloud interaction simulator (LACIS) (Hartmann et al., 2011), respectively, to observe immersion freezing of 300 nm mobility diameter selected kaolinite particles as a function of T and RH > 100 %. It is important to note that for both instruments, droplet freezing is not observed unlike previously discussed experiments but instead, the number of ice crystals are optically detected. Thus, f_{frz} is calculated from the ratio between observed ice crystal and aerosol numbers per volume of air. The model simulation parameter N_{tot} is derived from known experimental parameters, including residence time, $t_r = 5$ s, flow rate, $Q = 1.0$ L min^{-1}, and kaolinite particle concentrations, $N_p = 10$ cm^{-3} (Wex et al., 2014). By defining a single IFS over an interval of time equal to t_r, $N_{tot} = N_p Q t_r = 833$ particles per IFS. Similarly for LACIS, $Q = 0.08$ L min^{-1}, $t_r = 1.6$ s, and $N_{tot} = 21$ particles per IFS. Note that minimum f_{frz} values for CFDC and LACIS presented in Wex et al. (2014) are approximately equal to $1/N_{tot}$. We run 1440 and 6000 isothermal IFSs for IsoCFDC and IsoLACIS, respectively, equivalent to 2 h averages as done in Wex et al. (2014). J_{het} is taken from Knopf and Alpert (2013) for kaolinite IN. Simulation parameters for IsoCFDC and IsoLACIS are given in Table 1.

Figure 7 shows that simulated f_{frz} for IsoCFDC and IsoLACIS agree very well with CFDC and LACIS data by Wex et al. (2014). However, some data points fall outside of the 5 and 95 percentiles (Fig. 7a), which may imply that a greater uncertainty exists that cannot be explained by a stochastic freezing process. This may be due, in part, to uncertainty in ice crystal optical detection which is not accounted for in model simulations. The surface area for spherical 300 nm particles is $A_{300nm} = 2.8 \times 10^{-9}$ cm^2. However, the assumption that a kaolinite particle with an electrical mobility diameter of 300 nm is equal to a 300 nm diameter sphere is likely not true, due to shape irregularities, variable density, void fractions, multiple charges, and other geometries (DeCarlo et al., 2004; Slowik et al., 2004; Zelenyuk et al., 2006; Schmid et al., 2007; Park et al., 2008) with a tendency for greater surface area than assumed. Therefore, a distribution of particle surface area is expected and used in IsoCFDC and IsoLACIS with pa-

ACPD
15, 13109–13166, 2015

rameters $A_g = 6.2 \times 10^{-8}\,cm^2$ and $\sigma_g = 8.2$. These values were fitted to experimentally derived f_{frz}.

Calculations of $J_{het}^{apparent}$ and J_{het}^{actual} assuming constant ISA equal to A_{300nm} or accounting for variable ISA, respectively, in IsoCFDC and IsoLACIS are shown in Fig. 7b. We find excellent agreement between $J_{het}^{apparent}$ and data by Wex et al. (2014). Also, calculated J_{het}^{actual} are in agreement with J_{het} using the ABIFM for kaolinite in CFDC and LACIS experiments. J_{het} data by Wex et al. (2014) and data by Murray et al. (2011) and Pinti et al. (2012) disagree by 2 to 3.5 orders of magnitude. This is similar to the difference between $\overline{J}_{het}^{apparent}$ and $\overline{J}_{het}^{actual}$ likely due to A_g being 1.5 orders of magnitude larger than A_{300nm} and applying a surface area distribution. Furthermore, assuming that the electrical mobility diameter corresponds to the physical particle diameter and being spherical in geometry significantly overestimates ice nucleation kinetics, as demonstrated for IsoCFDC and IsoLACIS.

Wex et al. (2014) presented a detailed immersion freezing analysis of various kaolinite particle sizes and types of coatings, simulating all these cases is beyond the scope of this paper. However, we are certain that model simulations which use the same $J_{het}(T, a_w)$ will hold for all IN systems at all T and RH based solely on the fact that the same physical and statistical principles apply. In other words, prediction of immersion freezing kinetics (i.e. using J_{het}) in the simulations is independent of experimentally applied ISA, particle size, and particle coating type (assuming the coating dissolves when water is taken up and does not react with the IN surface). These findings demonstrate that the model simulations are applicable for ice nucleation studies using a CFDC and LACIS, and that data from Wex et al. (2014) support a time-dependent and stochastic immersion freezing process.

IFSs are used to describe AIDA chamber immersion freezing experiments applying natural dust IN by Niemand et al. (2012) in model simulations CrNI1 and CrNI2. Among the different types of natural dust investigated, we choose 2 Asian dust experiments at $-20.1 < T < -28.1\,^{\circ}C$ and $-14.3 < T < -22.4\,^{\circ}C$ (see ACI04_19 and ACI04_16 in Ta-

ACPD
15, 13109–13166, 2015

bles 2 and 3 in Niemand et al., 2012). A continuous non-linear cooling rate with time due to adiabatic expansion is fitted to experimental trajectories using a 4th order polynomial function. In AIDA experiments water saturation is typically reached after cooling begins. To mimic this process, ice particle production in model simulations is allowed after 80 s of cooling (see Fig. 2 in Niemand et al., 2012). Ice crystal concentration in an aerosol sampling flow of 5 L min^{-1}, from the chamber is observed every 5 s using an optical particle counter (Benz et al., 2005), thus a volume of 0.42 L of air is simulated. Total particles numbers in the simulated volume are on the order of 10^5 which agree well with minimum reported f_{frz} of about 10^{-5}. Niemand et al. (2012) reported lognormal surface-size distributions with parameters, $d_{S,median}$ and σ_g of polydisperse aerosol population. In CrNI1 and CrNI2, A_j is derived by sampling particle diameters from the corresponding number-size distributions and assuming spherical particles. Sampling stops when A_{tot} equals total surface area reported by Niemand et al. (2012). As previously discussed, assuming spherical particles results in a bias of $J_{het}(T)$, i.e. the slope of $J_{het}^{apparent}(T)$ is always underestimated (Fig. 4a). This assumption also underestimates total surface area resulting in erroneously high experimentally derived $J_{het}^{actual}(T)$ values compared with $J_{het}^{actual}(T)$ as demonstrated in Fig. 7b. Experimentally derived J_{het} is not available and so the ABIFM parameters m and c are fitted to experimentally derived f_{frz} data. Model simulation parameters for CrNI1 and CrNI2 are given in Table 2.

Figure 8 shows simulated f_{frz} and J_{het}^{actual} from CrNI1 and CrNI2 and the time evolution of simulated ice crystal concentration in CrNI1 observed during the experiments. Simulated f_{frz} (Fig. 8a) fall within the experimental uncertainty reported by Niemand et al. (2012) and the scatter in the data for all dust types. Narrow 5 and 95 % bounds are attributable to large N_{tot} on the order of 10^5 droplets per cooling simulation. Ice particle concentrations over time in CrNI1 are shown (insert in Fig. 8a) and are in excellent agreement with observations. It is important to note that ice crystal concentration data was not used for fitting parameters m and c. Figure 8b shows $\overline{J}_{het}^{actual}$ and upper and lower fiducial limits. As frozen fraction decreases the fiducial limits become broader

ACPD
15, 13109–13166, 2015

ranging from 0.8 to 2.5 orders of magnitude. We conclude that our model simulations are suitable for describing laboratory immersion freezing in AIDA cloud chamber and further support the necessity of quantification of ISA variability in the derivation of ice nucleation kinetics.

Notice that in Fig. 8a, the vertical scatter in the experimental data increases at warmer T and for low f_{frz}, which implies that uncertainty likely increases as f_{frz} decreases. Since aerosol numbers and surface area in the experiments by Niemand et al. (2012) are relatively the same for all experiments, decreasing f_{frz} implies fewer detected ice crystals or decreasing numbers of ice nucleation events resulting in an increase in experimental uncertainty. A deterministic (singular) approach for interpretation and analysis of ice crystal production, which inherently ignores stochastic freezing, cannot explain the increase in the data scatter for smaller f_{frz} values at warmer T. These observations can only be explained by a stochastic and time-dependent immersion freezing process. The fiducial limits of J_{het}^{actual} shown in Fig. 8b, in fact, capture this effect of larger scatter as T increases implying the uncertainty in observed ice nucleation kinetics increases. Since the freezing efficiency of Asian dust was shown to be similar for Saharan, Canary Island, and Israeli dust (Niemand et al., 2012), the new ABIFM parameterization of $J_{het}(T, a_w)$ derived here is applicable for natural dust.

4 Simulation findings and uncertainty analysis

Our results strongly suggest that laboratory immersion freezing studies should provide accurate estimates of ISA variability in droplets. We find that simplified assumptions about ISA can result in misinterpretation and miscalculation of J_{het} values. This includes assuming identical surface area, which implicitly imposes a dependence of J_{het} on both ISA and r. Future laboratory immersion freezing studies should also consider the stochastic nature of ice nucleation following CNT and resulting uncertainties. When only a single ice nucleation experiment is performed or too few droplets are used, statistical uncertainty can potentially be very large and may limit data interpretation. The

ACPD
15, 13109–13166, 2015

surface area based deterministic approach deriving $n_s(T)$ is an alternative to calculating J_{het}, but does not consider stochastic effects or effect of time in analysis of immersion freezing. By design, $n_s(T)$ should therefore, not have any dependence on r. However, this is not supported as $n_s(T)$ has been observed to be dependent on r for feldspar and kaolinite (Herbert et al., 2014).

The model simulation and laboratory data sets investigated here were performed for IN immersed in pure water droplets. However, aqueous solution droplets having $a_w < 1.0$ are frequently present in the atmosphere at supercooled temperatures and subsaturated conditions (i.e. RH < 100 %). The ABIFM (Eqs. 4–6) inherently and accurately accounts for these conditions and thus, provides a complete description of immersion freezing for laboratory experiments, as well as cloud models under atmospherically relevant T and RH. ABIFM is independent of the nature of the solute, and therefore, it can be applied in the exact same way to immersion freezing of pure water ($a_w = 1.0$) or aqueous solution ($a_w < 1.0$). We suggest that future isothermal and cooling rate dependent immersion freezing studies investigate aqueous solution droplets in addition to water droplets (e.g. Archuleta et al., 2005; Alpert et al., 2011b; Wex et al., 2014), providing additional data sets to constrain ice nucleation kinetics and to validate and expand ABIFM and other parameterizations.

Uncertainty analysis is crucial for the interpretation of laboratory immersion freezing results. Here we present a quantitative uncertainty analysis of J_{het}, by defining ΔJ_{het} as the total uncertainty derived from individual contributions of stochastic uncertainty due to N_{tot}, temperature accuracy referred to as ΔT, a_w or RH accuracy referred to as ΔRH, ISA variability expressed as σ_g, and accuracy of measuring absolute surface area referred to as ΔA_g. This uncertainty analysis is applicable to both isothermal and cooling rate dependent immersion freezing experiments. It is convenient to quantify ΔJ_{het} in the form of a $\overset{\times}{\div}$ error instead of a typical ± error due to J_{het} varying exponentially over a linear range in T. If $J_{het} = 100\,\mathrm{cm^{-2}\,s^{-1}}$ with a factor of ±3 error for example, then $\Delta J_{het} = \overset{\times}{\div}3$ equivalent to $J_{het} = 100^{\times 3}_{\div 3} = 100^{+200}_{-67}\,\mathrm{cm^{-2}\,s^{-1}}$. In the following analysis, ΔJ_{het} is quantified as $\overset{\times}{\div}$, representing a factor error.

ACPD
15, 13109–13166, 2015

The uncertainty due to stochastic freezing is derived by running 10^5 IFSs with different values of N_{tot} and calculating ΔJ_{het} where the widths of the fiducial limits are smallest, i.e. at $f_{frz} \simeq 0.5$. Thus, ΔJ_{het} derived from N_{tot} yields the smallest error estimate possible or the limit of greatest experimental accuracy. Figure 9a illustrates that smaller N_{tot} results in larger ΔJ_{het}. When $N_{tot} = 30$ for example, $\Delta J_{het} = {}^{\times 15}_{\div 5}$, and when $N_{tot} = 1000$, $\Delta J_{het} = {}^{\times 1.3}_{\div 1.3}$. The uncertainty contribution due to ΔT is calculated using the slope of J_{het} vs. T following a similar procedure as in Riechers et al. (2013). Using the ABIFM at various temperature ranges and for different IN types (Knopf and Alpert, 2013), J_{het} varies by a factor of 7.5 ± 5.5 per degree K. This means that if $\Delta T = \pm 1.0$ K, $\Delta J_{het} = {}^{\times}_{\div} 7.5$ on average, but can be ${}^{\times}_{\div} 2$ or ${}^{\times}_{\div} 13$ depending on the IN type and the range in T and RH. For example, $\Delta T = \pm 0.5$ K translates to $\Delta J_{het} = {}^{\times}_{\div} 3.75$ as displayed in Fig. 9a. Considering the uncertainty in RH, Eq. (4) is used to derive $\Delta J_{het} = J_{het}(\Delta a_w)/J_{het}(\Delta a_w \pm \Delta \mathrm{RH}) = 10^{m \Delta \mathrm{RH}}$. Values of m in Eq. (4) are taken from this study and from Knopf and Alpert (2013) ranging from 15–123 and results in 69 on average. The mean and range of ΔJ_{het} due to ΔRH are shown in Fig. 9b. For example, if $\Delta \mathrm{RH} = \pm 3\,\%$, then $\Delta J_{het} = {}^{\times}_{\div} 117$ on average. If ISA per droplet varies in an experiment, but is assumed to be uniform, J_{het} is overestimated for $f_{frz} < 0.5$ and underestimated for $f_{frz} > 0.5$. This effect is quantified by allowing σ_g to vary and calculating the ratio $\Delta J_{het} = \overline{J}^{\mathrm{apparent}}_{het} / \overline{J}^{\mathrm{actual}}_{het}$ evaluated at $f_{frz} = 0.1$ and 0.9. The resulting ΔJ_{het} is displayed in Fig. 9c as a function of σ_g. If $\sigma_g = 10$, for example, then $\Delta J_{het} = {}^{\times 4}_{\div 20}$ at $f_{frz} = 0.1$ and 0.9. Finally, ΔJ_{het} is directly proportional to ΔA_g shown in Fig. 9c, e.g. if $\Delta A_g = {}^{\times}_{\div} 5$, then $\Delta J_{het} = {}^{\times}_{\div} 5$.

Figure 9 demonstrates that each experimental parameter contributes to the uncertainty in J_{het}. The total uncertainty in J_{het} can then be estimated by summing the error contributions due to N_{tot}, T, RH, σ_g, and A_g, respectively. Figure 9 shows dotted lines serving as example values of experimental uncertainties and corresponding ΔJ_{het}. Applying $N_{tot} = 30$, $\Delta T = \pm 0.5$ K, $\Delta \mathrm{RH} = \pm 3\,\%$, $\sigma_g = 10$, and $\Delta A_g = {}^{\times}_{\div} 5$, results in $\Delta J_{het} = {}^{\times 148}_{\div 154}$. If laboratory immersion freezing studies were to be conducted under these

ACPD
15, 13109–13166, 2015

conditions, then the range in experimentally derived J_{het} should be over 4 orders of magnitude. Notice that the uncertainty due to RH alone can potentially dominate the total uncertainty. We hope that Fig. 9 provides guidance in conducting future immersion freezing studies.

We test our analysis to reproduce experimentally derived uncertainty. In Knopf and Alpert (2013), all experimentally derived J_{het} fell within ±2 orders of magnitude as a function of the a_w criterion (Eq. 5) and as a result, this range was adapted as a conservative uncertainty estimate for the ABIFM model. The root mean square error of over 18 000 droplet freezing events for 6 different IN types was experimentally derived independent from model simulations, as an alternative uncertainty estimate exhibiting values as high as ±1.3 orders of magnitude. Experimental parameters of studies used in the formulation of the ABIFM for pure water and aqueous solution droplets (Alpert et al., 2011a, b; Knopf and Forrester, 2011; Rigg et al., 2013; Knopf and Alpert, 2013) were about $N_{tot} = 300$, $\Delta T = \pm 0.3\,\mathrm{K}$, $\Delta\mathrm{RH} = \pm 1\,\%$, $\sigma_g = 5$, and $\Delta A_g = \overset{\times}{\div} 5$. Applying the analysis displayed in Fig. 9 results in an uncertainty of $\Delta J_{het} = \overset{\times 16}{\div 18}$ (spanning about 2.5 orders of magnitude) for the ABIFM model. This estimate is in excellent agreement with independently derived root mean square errors of J_{het} (Knopf and Alpert, 2013) and demonstrates the accuracy of our uncertainty analysis.

Model simulations reproduced observations of immersion freezing due to the IN illite by Diehl et al. (2014) and Broadley et al. (2012). These experimental data were included in a recent intercomparison study of illite IN immersion freezing by Hiranuma et al. (2015). Using 17 different instruments, experimentally derived $n_s(T)$ values were observed to increase from 10^{-3} to $10^{8}\,\mathrm{cm}^{-2}$ when T decreased from 263 to 236 K, equivalent to a slope of 0.5 orders of magnitude per 1 K. The instruments used are grouped by common methods and include, (i) cold stage (Broadley et al., 2012; Bingemer et al., 2012; Schill and Tolbert, 2013; Wright and Petters, 2013; O'Sullivan et al., 2014; Budke and Koop, 2015), (ii) liquid aliquots (Hill et al., 2014), (iii) droplet levitation (Szakáll et al., 2009; Diehl et al., 2014; Hoffmann et al., 2013), (iv) cloud chamber (Möhler et al., 2003; Niemand et al., 2012; Tajiri et al., 2013) and (v) continuous flow

ACPD
15, 13109–13166, 2015

(Bundke et al., 2008; Stetzer et al., 2008; Welti et al., 2009; Lüönd et al., 2010; Chou et al., 2011; Friedman et al., 2011; Hartmann et al., 2011; Kanji et al., 2013; Tobo et al., 2013; Wex et al., 2014). The scatter in the n_s is roughly 3 orders of magnitude, but depending on T, a n_s range of 2 and 4 orders of magnitude can envelop the data. However, the authors provided no quantitative uncertainty analysis to explain this scatter. Since experimental methods and data reproduced by presented model simulations are included in Hiranuma et al. (2015) for illite, we apply the quantitative uncertainty analysis presented in Fig. 9 to provide a potential explanation of the data scatter. Although, J_{het} and $n_s(T)$ are different quantities, the contribution to their uncertainties is the same for ΔT, ΔRH, σ_g, ΔA_g.

Experimental T uncertainty for all methods typically ranged from ±0.2 to ±1.0 K, and hence $\Delta T = \pm 0.5$ is chosen as a representative value. Considering the slope n_s vs. T, $\Delta T = \pm 0.5$ contributes a factor of ∼ 2 uncertainty to $n_s(T)$, or $\Delta n_s = {}^{\times}_{\div} 2$. The ISA distribution width parameter of simulated experiments (Tables 1 and 2) is averaged to represent $n_s(T)$ data, yielding a reasonable value of $\sigma_g = 7$, resulting in $\Delta n_s = {}^{\times 3}_{\div 12}$. The ISA measurement error is considered to be $\Delta A_g = {}^{\times}_{\div} 5$, thus $\Delta n_s = {}^{\times}_{\div} 5$. Calculation of $n_s(T)$ is not stochastic by design, and thus any uncertainty contribution due to N_{tot} on $n_s(T)$ was previously not considered (Hiranuma et al., 2015). Additionally, the intercomparison analysis ignores differences in experimental time scales in $n_s(T)$ derivation. However, this study demonstrates that the stochastic uncertainty can explain most immersion freezing data and therefore, likely contributes to the range of data scatter in $n_s(T)$. Typically, N_{tot} is about 50 which serves as a reasonable representation yielding $\Delta n_s = {}^{\times 8}_{\div 4}$, although N_{tot} can vary between 10 and 1000 depending on the experiment. Previous immersion freezing experiments for illite IN have shown that when r or residence time differ by 1 order of magnitude, freezing temperatures shift by about 0.75 K on average (Broadley et al., 2012; Welti et al., 2012; Knopf and Alpert, 2013). As discussed in Hiranuma et al. (2015), cooling rates and residence times in the different instruments varied over ±2 orders of magnitude, or $\Delta t = {}^{\times}_{\div} 100$, corresponding to $\Delta T = \pm 1.5$ K, and thus contributing to an error of ±0.75 orders of magnitude or $\Delta n_s = {}^{\times}_{\div} 6$. Accounting for

ACPD
15, 13109–13166, 2015

all uncertainties and making use of Fig. 9 results in $\Delta n_s = {}^{\times(2+3+5+8+6)}_{\div(2+12+5+4+6)}$ for a total uncertainty of $\Delta n_s = {}^{\times 24}_{\div 29}$, or an uncertainty range of 2.8 orders of magnitude. The vast majority of data in Hiranuma et al. (2015) fall within this uncertainty and implies that variability in $n_s(T)$ can be attributed to experimental, time-dependent, and stochastic uncertainties. It is important to note that the uncertainty due to neglecting time, ISA variability and stochastic effect contributes more to Δn_s, than T and ISA measurement error. Hiranuma et al. (2015) hypothesized that experimental procedures of droplet or particle preparation, including particle generation, size selection, ice crystal detection, particle loss at instrument sampling inlets, contamination, inhomogeneous temperature, and differences in surface cation concentration between wet dispersed or dry dispersed particles may be the cause in measured scatter in $n_s(T)$ data. These effects are not considered in the uncertainty analysis presented here, but may also contribute.

5 Atmospheric implications

The model simulations presented here are used to investigate effects of variable ISA on atmospheric ice nucleation. Only immersion freezing is considered, however, mixed-phase and cirrus clouds can undergo other cloud microphysical effects such as homogeneous ice nucleation, deposition ice nucleation, contact ice nucleation, ice multiplication, ice crystal growth, water vapour depletion due to the Bergeron–Wegener–Findeisen process, entrainment and mixing, and ice crystal sedimentation. The purpose here is not to simulate any physically realistic cloud, but to investigate the sensitivity of ice particle production on σ_g. In 2 model simulations MPC1 and MPC2, IN particle diameters, D_p, are either uniform or sampled from a lognormal distribution, respectively. Parameters are given in Table 2. Surface area is calculated assuming spherical particles. We apply illite particles as IN with $N_p = 100\,\mathrm{cm}^{-3}$ (air). Mixed-phase cloud conditions are assumed in which one particle is immersed inside of one dilute cloud droplet with $a_w \sim 1.0$.

ACPD
15, 13109–13166, 2015

Figure 10 presents the results of MPC1 and MPC2 applying $N_{tot} = 10^7$ illite particles in 100 L of air with an updraft velocity, $w = 100\,cm\,s^{-1}$, as a function of T, t, and height, h, where the first ice nucleation event occurs at $t = 0$ and $h = 0$. Simulated f_{frz} curves are shown in Fig. 10a, in addition to J_{het} and the ice saturation ratio, S_{ice}, as a function of T. As T decreases and t increases, J_{het}, S_{ice} and f_{frz} increase. Corresponding ice crystal concentrations derived using MPC1 and MPC2 are displayed in Fig. 10b as the number of ice crystals formed per volume of air. Although homogeneous ice nucleation of droplets is not considered in the model, the temperature range in which this process becomes important is shaded in gray.

Values of f_{frz} derived in MPC2 are larger than for MPC1 and extend over a wider range of T as shown in Fig. 10a. As a result, the onset of ice nucleation, which occurs at $f_{frz} = 10^{-7}$ (or 10^{-2} ice crystals L^{-1}), is about 5 K warmer for MPC2 compared to MPC1 (Fig. 10a). Typical ice crystal concentrations observed in Arctic mixed-phase clouds can range from 0.01–10 L^{-1} (air) at temperatures warmer than the homogeneous freezing limit $235 < T < 273.15$ K (McFarquhar et al., 2007; Prenni et al., 2009; Lance et al., 2011). The model presented here which accounts for ISA variability achieves similar ice crystal concentrations between 251–258 K as demonstrated in Fig. 10b. Our calculations indicate that onset ice nucleation in mixed-phase clouds may be significantly influenced by a polydispersed atmospheric aerosol population. It can be expected that atmospheric ice crystals are produced across a broad range of temperatures, even at $T \geq -15\,^{\circ}C$. Furthermore, this result underscores the importance of determining coarse mode aerosol particle numbers and total particle surface areas to improve our predictive understanding of atmospheric ice formation (Knopf et al., 2014).

6 Summary and conclusions

Immersion freezing simulations based on a droplet resolved stochastic ice nucleation process applicable for various types of IN and experiments are presented here for both isothermal conditions and applying a cooling rate, r. The parameters in the IFSs are all

ACPD
15, 13109–13166, 2015

physically defined and measurable, including heterogeneous ice nucleation rate coefficients, J_{het}, the number of droplets at the start of an experiment, N_{tot}, the average ISA, A_g, and the variability of ISA, σ_g, which is assumed to be lognormally distributed due to employed IN particle preparation and droplet generation. Alternatively, individually measured ISA per droplets can be used. For IFSs in which a cooling rate, r, is applied, J_{het} as a function of T and aqueous solution water activity, a_w, can be calculated following the water activity based immersion freezing model (ABIFM) applicable for both pure water ($a_w = 1.0$) and aqueous solution ($a_w < 1.0$) droplets. These IFSs generate frozen and unfrozen droplet fraction data, f_{ufz} and f_{frz}, respectively, and using a Monte Carlo method in which 10^5 IFSs are performed under the same conditions, 5 and 95 % bounds are derived as uncertainty estimates.

The sensitivity of f_{ufz} on σ_g and N_{tot} was tested using sets of isothermal IFSs, where a single set is referred to as a model simulation. Uniform ISA (i.e. $\sigma_g = 1$) resulted in f_{ufz} (on a logarithmic scale) being linear with t. When ISA varied lognormally with parameters $\mu = \ln(A_g)$ and $\sigma = \ln(\sigma_g)$, where $\sigma_g > 1$, $\ln(f_{ufz})$ vs. t exhibit non-linear behavior. When larger or smaller N_{tot} was used, f_{ufz} had a smaller and larger uncertainty, respectively, due to the statistical significance of observing more freezing events. Effects of σ_g and N_{tot} on f_{ufz} are independent and thus, can be quantified apart from each other. These results demonstrate that in laboratory immersion freezing experiments, variable ISA imposes changes in trajectories of f_{ufz} and f_{frz} over time, and that the number of investigated droplets significantly impacts experimental uncertainty.

Cooling rate model simulations were used to test the validity of assuming uniform ISA. This was accomplished by recalculating J_{het} after simulation of immersion freezing in two ways, either (i) assuming uniform ISA referred to as the "apparent" ice nucleation rate coefficient, $J_{het}^{apparent}$, or (ii) accounting for variable ISA referred to as the "actual" ice nucleation rate coefficient, J_{het}^{actual}. When different r were applied in simulations, values of $J_{het}^{apparent}$ were significantly different from each other. When comparing experiments with different ISA but identical r, $J_{het}^{apparent}(T)$ was again significantly dif-

ACPD
15, 13109–13166, 2015

ferent. For $f_{frz} < 0.5$ and $f_{frz} > 0.5$, $J_{het}^{apparent}$ was over and underestimated, respectively, compared to J_{het}^{actual}, yielding an erroneous slope of $J_{het}^{apparent}(T)$. These results demonstrate that the assumption of identical ISA implicitly imposes a cooling rate and surface area dependence on experimentally derived $J_{het}(T)$. However, derivation of J_{het}^{actual} from model simulations accounting for variable ISA were consistent for different r and ISA, supporting a stochastic immersion freezing description as predicted by CNT.

Model simulations in which variable ISA was considered reproduced laboratory experiments using Arizona test dust (ATD) (Wright and Petters, 2013), illite (Broadley et al., 2012; Diehl et al., 2014), kaolinite (Wex et al., 2014; Herbert et al., 2014), feldspar (Herbert et al., 2014), and natural dusts from Asia, Israel, the Sahara desert and Canary Islands (Niemand et al., 2012) acting as IN. Despite whether isothermal or linear and nonlinear cooling rates were applied, modeled and experimental f_{frz} and f_{ufz} were in agreement within the stochastic uncertainty. More importantly, experimentally derived $J_{het}(T)$ and simulated $J_{het}^{apparent}$ were in agreement, indicating an imposed bias solely due to the assumption of uniform ISA and not to physical processes governing ice nucleation. Despite this fact, model simulations can correct for this introduced bias yielding "actual" values, or J_{het}^{actual}, which resulted in consistent agreement between different studies and additionally new a_w based parameterizations of $J_{het}(\Delta a_w)$ for feldspar and natural dusts.

A quantitative uncertainty analysis of J_{het} was presented applicable for experimental studies in which the contribution due to (i) N_{tot}, (ii) temperature accuracy referred to as ΔT, (iii) a_w or RH accuracy referred to as ΔRH, (iv) σ_g, and (v) the accuracy of A_g referred to as ΔA_g, were individually quantified. The following points summarize these error sources and give recommendations for future experimental studies:

– Applying too few N_{tot} or performing only a single ice nucleation experiment in laboratory studies results in highly uncertain freezing results. Therefore, repetition of immersion freezing experiments or a statistically significant number of droplets must be applied. We recommend using at least 100 droplets and three indepen-

ACPD
15, 13109–13166, 2015

dent freezing cycles in order to better quantify data scatter and average J_{het}, f_{frz}, and f_{ufz} values. This contributes to a range of 0.75 orders of magnitude in the uncertainty of experimentally derived J_{het}.

– For different IN types, the slope of J_{het} vs. T is not the same and thus, the uncertainty due to ΔT is IN type dependent, but can be as high as 1 order of magnitude per 1 K. We recommended that ΔT remain $< \pm 0.5$ K to achieve an acceptable uncertainty contribution, i.e. half an order of magnitude.

– The greatest source of error stems from RH, or ΔRH. Immersion freezing experiments for RH < 100 % should aim for ΔRH to be as small as possible. Current and future immersion freezing experiments should be designed to carefully control RH and quantify its uncertainty.

– Droplets in laboratory immersion freezing experiments will not have identical ISA, but will vary from droplet to droplet (σ_g) around some ISA value (A_g). Variability in ISA and corresponding uncertainty should be quantified and accounted for when analyzing ice nucleation experiments.

– Surface area and nucleation time scales clearly affect immersion freezing data. Common assumptions of ISA and neglecting the impact of variable experimental time scales will lead to an incomplete experimental accuracy and uncertainty. Consideration of these effects is recommended to narrow the uncertainty in predicting ice crystal formation.

The influence of variable ISA on ice crystal production in an idealized cloud model was investigated using two IFSs having $\sigma_g = 1$ and 5 (i.e. monodisperse and polydisperse IN populations, respectively). Ice nucleation occurred over a broader range of time and temperature resulting in greater ice particle production for $\sigma_g = 5$. Ice crystal concentrations, N_{ice}, in the range of 0.01–100 L^{-1} (air) consistently occurred at temperatures about 5 K warmer when applying polydispersed IN populations compared to

ACPD
15, 13109–13166, 2015

IFSs of monodispersed IN. Likewise, at a constant T, N_{ice} were consistently greater by two orders of magnitude. This implies that field measurements should determine and consider the entire aerosol size distribution as a source of IN.

These findings have significant implications for analysis and interpretation of immersion freezing data. We suggest that ice nucleation experiments and field studies focus on the effect of particle surface area and nucleation time for further validation of presented analyses and improvement of our predictive understanding of atmospheric ice formation. Laboratory derived J_{het} values can greatly aid in interpretation of atmospheric ice nucleation due to the fact that this parameter allows extrapolation to time scales and IN surface areas experienced in the atmosphere. A very simple stochastic freezing model based on a binomial distribution in accordance with classical nucleation theory, can reconcile immersion freezing data for various IN types and measurement techniques when the applied IN surface areas are treated more realistically. These findings hopefully stimulate further discussion on the analytical procedure and interpretation of immersion freezing and its implementation in atmospheric cloud and climate models.

Acknowledgements. This research was supported by the U.S. Department of Energy, Office of Science (BER), under Award Number DE-SC0008613.

References

Alpert, P. A., Aller, J. Y., and Knopf, D. A.: Ice nucleation from aqueous NaCl droplets with and without marine diatoms, Atmos. Chem. Phys., 11, 5539–5555, doi:10.5194/acp-11-5539-2011, 2011a. 13113, 13138

Alpert, P. A., Knopf, D. A., and Aller, J. Y.: Initiation of the ice phase by marine biogenic surfaces in supersaturated gas and supercooled aqueous phases, Phys. Chem. Chem. Phys., 13, 19882–19894, doi:10.1039/c1cp21844a, 2011b. 13113, 13136, 13138

Archuleta, C. M., DeMott, P. J., and Kreidenweis, S. M.: Ice nucleation by surrogates for atmospheric mineral dust and mineral dust/sulfate particles at cirrus temperatures, Atmos. Chem. Phys., 5, 2617–2634, doi:10.5194/acp-5-2617-2005, 2005. 13113, 13114, 13136

ACPD
15, 13109–13166, 2015

Baker, M. B.: Cloud microphysics and climate, Science, 276, 1072–1078, doi:10.1126/science.276.5315.1072, 1997. 13111

Bedjanian, Y., Romanias, M. N., and El Zein, A.: Uptake of HO_2 radicals on Arizona Test Dust, Atmos. Chem. Phys., 13, 6461–6471, doi:10.5194/acp-13-6461-2013, 2013. 13122

Benz, S., Megahed, K., Möhler, O., Saathoff, H., Wagner, R., and Schurath, U.: T-dependent rate measurements of homogeneous ice nucleation in cloud droplets using a large atmospheric simulation chamber, J. Photoch. Photobio. A, 176, 208–217, doi:10.1016/j.jphotochem.2005.08.026, 2005. 13134

Bingemer, H., Klein, H., Ebert, M., Haunold, W., Bundke, U., Herrmann, T., Kandler, K., Müller-Ebert, D., Weinbruch, S., Judt, A., Wéber, A., Nillius, B., Ardon-Dryer, K., Levin, Z., and Curtius, J.: Atmospheric ice nuclei in the Eyjafjallajökull volcanic ash plume, Atmos. Chem. Phys., 12, 857–867, doi:10.5194/acp-12-857-2012, 2012. 13138

Boucher, O., Randall, D., Artaxo, P., Bretherton, C., Feingold, G., Forster, P., Kerminen, V.-M., Kondo, Y., Liao, H., Lohmann, U., Rasch, P., Satheesh, S. K., Sherwood, S., Stevens, B. and Zhang, X. Y.: Clouds and aerosols, chapt. 7, in: Climate Change 2013: The Physical Science Basis. Contribution of Working Group I to the Fifth Assessment Report of the Intergovernmental Panel on Climate Change, Cambridge University Press, Cambridge, UK and New York, NY, USA, 571–657, 2013. 13111

Broadley, S. L., Murray, B. J., Herbert, R. J., Atkinson, J. D., Dobbie, S., Malkin, T. L., Condliffe, E., and Neve, L.: Immersion mode heterogeneous ice nucleation by an illite rich powder representative of atmospheric mineral dust, Atmos. Chem. Phys., 12, 287–307, doi:10.5194/acp-12-287-2012, 2012. 13113, 13114, 13118, 13123, 13124, 13130, 13138, 13139, 13143, 13158

Brunauer, S., Emmett, P. H., and Teller, E.: Adsorption of gases in multimolecular layers, J. Am. Chem. Soc., 60, 309–319, doi:10.1021/ja01269a023, 1938. 13122

Budke, C. and Koop, T.: BINARY: an optical freezing array for assessing temperature and time dependence of heterogeneous ice nucleation, Atmos. Meas. Tech., 8, 689–703, doi:10.5194/amt-8-689-2015, 2015. 13138

Bundke, U., Nillius, B., Jaenicke, R., Wetter, T., Klein, H., and Bingemer, H.: The fast ice nucleus chamber, FINCH, Atmos. Res., 90, 180–186, doi:10.1016/j.atmosres.2008.02.008, 2008. 13139

Chen, T., Rossow, W. B., and Zhang, Y. C.: Radiative effects of cloud-type variations, Tellus A, 50, 259–264, doi:10.1175/1520-0442(2000)013<0264:REOCTV>2.0.CO;2, 2000. 13111

ACPD
15, 13109–13166, 2015

Chou, C., Stetzer, O., Weingartner, E., Jurányi, Z., Kanji, Z. A., and Lohmann, U.: Ice nuclei properties within a Saharan dust event at the Jungfraujoch in the Swiss Alps, Atmos. Chem. Phys., 11, 4725–4738, doi:10.5194/acp-11-4725-2011, 2011. 13139

Connolly, P. J., Möhler, O., Field, P. R., Saathoff, H., Burgess, R., Choularton, T., and Gallagher, M.: Studies of heterogeneous freezing by three different desert dust samples, Atmos. Chem. Phys., 9, 2805–2824, doi:10.5194/acp-9-2805-2009, 2009. 13113

DeCarlo, P. F., Slowik, J. G., Worsnop, D. R., Davidovits, P., and Jimenez, J. L.: Particle morphology and density characterization by combined mobility and aerodynamic diameter measurements. Part 1: Theory, Aerosol Sci. Tech., 38, 1185–1205, doi:10.1080/027868290903907, 2004. 13114, 13132

DeMott, P. J., Prenni, A. J., Liu, X., Kreidenweis, S. M., Petters, M. D., Twohy, C. H., Richardson, M. S., Eidhammer, T., and Rogers, D. C.: Predicting global atmospheric ice nuclei distributions and their impacts on climate, P. Natl. Acad. Sci. USA, 107, 11217–11222, doi:10.1073/pnas.0910818107, 2010. 13113, 13132

Diehl, K., Debertshäuser, M., Eppers, O., Schmithüsen, H., Mitra, S. K., and Borrmann, S.: Particle surface area dependence of mineral dust in immersion freezing mode: investigations with freely suspended drops in an acoustic levitator and a vertical wind tunnel, Atmos. Chem. Phys., 14, 12343–12355, doi:10.5194/acp-14-12343-2014, 2014. 13114, 13125, 13130, 13131, 13138, 13143, 13156, 13159, 13162

Friedman, B., Kulkarni, G., Beránek, J., Zelenyuk, A., Thornton, J. A., and Cziczo, D. J.: Ice nucleation and droplet formation by bare and coated soot particles, J. Geophys. Res., 116, D17203, doi:10.1029/2011JD015999, 2011. 13139

Haag, W., Kärcher, B., Ström, J., Minikin, A., Lohmann, U., Ovarlez, J., and Stohl, A.: Freezing thresholds and cirrus cloud formation mechanisms inferred from in situ measurements of relative humidity, Atmos. Chem. Phys., 3, 1791–1806, doi:10.5194/acp-3-1791-2003, 2003. 13111

Hartmann, S., Niedermeier, D., Voigtländer, J., Clauss, T., Shaw, R. A., Wex, H., Kiselev, A., and Stratmann, F.: Homogeneous and heterogeneous ice nucleation at LACIS: operating principle and theoretical studies, Atmos. Chem. Phys., 11, 1753–1767, doi:10.5194/acp-11-1753-2011, 2011. 13132, 13139

Hegg, D. A. and Baker, M. B.: Nucleation in the atmosphere, Rep. Prog. Phys., 72, 056801, doi:10.1088/0034-4885/72/5/056801, 2009. 13111

ACPD
15, 13109–13166, 2015

Herbert, R. J., Murray, B. J., Whale, T. F., Dobbie, S. J., and Atkinson, J. D.: Representing time-dependent freezing behaviour in immersion mode ice nucleation, Atmos. Chem. Phys., 14, 8501–8520, doi:10.5194/acp-14-8501-2014, 2014. 13114, 13118, 13123, 13124, 13125, 13128, 13129, 13136, 13143, 13158, 13161

Hill, T. C. J., Moffett, B. F., DeMott, P. J., Georgakopoulosd, D. G., Stumpa, W. L., and Franca, G. D.: Measurement of ice nucleation-active bacteria on plants and in precipitation by quantitative PCR, Appl. Environ. Microb., 80, 1256–1267, doi:10.1128/AEM.02967-13, 2014. 13138

Hiranuma, N., Augustin-Bauditz, S., Bingemer, H., Budke, C., Curtius, J., Danielczok, A., Diehl, K., Dreischmeier, K., Ebert, M., Frank, F., Hoffmann, N., Kandler, K., Kiselev, A., Koop, T., Leisner, T., Möhler, O., Nillius, B., Peckhaus, A., Rose, D., Weinbruch, S., Wex, H., Boose, Y., DeMott, P. J., Hader, J. D., Hill, T. C. J., Kanji, Z. A., Kulkarni, G., Levin, E. J. T., McCluskey, C. S., Murakami, M., Murray, B. J., Niedermeier, D., Petters, M. D., O'Sullivan, D., Saito, A., Schill, G. P., Tajiri, T., Tolbert, M. A., Welti, A., Whale, T. F., Wright, T. P., and Yamashita, K.: A comprehensive laboratory study on the immersion freezing behavior of illite NX particles: a comparison of 17 ice nucleation measurement techniques, Atmos. Chem. Phys., 15, 2489–2518, doi:10.5194/acp-15-2489-2015, 2015. 13113, 13138, 13139, 13140

Hoffmann, N., Duft, D., Kiselev, A., and Leisner, T.: Contact freezing efficiency of mineral dust aerosols studied in an electrodynamic balance: quantitative size and temperature dependence for illite particles, Faraday Discuss., 165, 383–390, doi:10.1039/C3FD00033H, 2013. 13138

Hoose, C. and Möhler, O.: Heterogeneous ice nucleation on atmospheric aerosols: a review of results from laboratory experiments, Atmos. Chem. Phys., 12, 9817–9854, doi:10.5194/acp-12-9817-2012, 2012. 13113, 13131

Iannone, R., Chernoff, D. I., Pringle, A., Martin, S. T., and Bertram, A. K.: The ice nucleation ability of one of the most abundant types of fungal spores found in the atmosphere, Atmos. Chem. Phys., 11, 1191–1201, doi:10.5194/acp-11-1191-2011, 2011. 13113

Kanji, Z. A., Welti, A., Chou, C., Stetzer, O., and Lohmann, U.: Laboratory studies of immersion and deposition mode ice nucleation of ozone aged mineral dust particles, Atmos. Chem. Phys., 13, 9097–9118, doi:10.5194/acp-13-9097-2013, 2013. 13139

Knopf, D. A. and Alpert, P. A.: A water activity based model of heterogeneous ice nucleation kinetics for freezing of water and aqueous solution droplets, Faraday Discuss., 165, 513–

ACPD
15, 13109–13166, 2015

534, doi:10.1039/c3fd00035d, 2013. 13112, 13113, 13114, 13118, 13120, 13122, 13127, 13130, 13131, 13132, 13137, 13138, 13139, 13155, 13160, 13161, 13162, 13163, 13166

Knopf, D. A. and Forrester, S.: Freezing of water and aqueous NaCl droplets coated by organic monolayers as a function of surfactant properties and water activity, J. Phys. Chem. A, 115, 5579–5591, doi:10.1021/jp2014644, 2011. 13113, 13138

Knopf, D. A., Alpert, P. A., Wang, B., O'Brien, R. E., Kelly, S. T., Laskin, A., Gilles, M. K., and Moffet, R. C.: Microspectroscopic imaging and characterization of individually identified ice nucleating particles from a case field study, J. Geophy. Res., 119, 10365–10381, doi:10.1002/2014JD021866, 2014. 13141

Koop, T. and Zobrist, B.: Parameterizations for ice nucleation in biological and atmospheric systems, Phys. Chem. Chem. Phys., 11, 10839–10850, doi:10.1039/B914289D, 2009. 13114

Koop, T., Luo, B. P., Biermann, U. M., Crutzen, P. J., and Peter, T.: Freezing of $HNO_3/H_2SO_4/H_2O$ solutions at stratospheric temperatures: nucleation statistics and experiments, J. Phys. Chem. A, 101, 1117–1133, doi:10.1021/jp9626531, 1997. 13116, 13127

Koop, T., Luo, B. P., Tsias, A., and Peter, T.: Water activity as the determinant for homogeneous ice nucleation in aqueous solutions, Nature, 406, 611–614, doi:10.1038/35020537, 2000. 13112, 13118

Kulkarni, G., Fan, J., Comstock, J. M., Liu, X., and Ovchinnikov, M.: Laboratory measurements and model sensitivity studies of dust deposition ice nucleation, Atmos. Chem. Phys., 12, 7295–7308, doi:10.5194/acp-12-7295-2012, 2012. 13114

Lance, S., Shupe, M. D., Feingold, G., Brock, C. A., Cozic, J., Holloway, J. S., Moore, R. H., Nenes, A., Schwarz, J. P., Spackman, J. R., Froyd, K. D., Murphy, D. M., Brioude, J., Cooper, O. R., Stohl, A., and Burkhart, J. F.: Cloud condensation nuclei as a modulator of ice processes in Arctic mixed-phase clouds, Atmos. Chem. Phys., 11, 8003–8015, doi:10.5194/acp-11-8003-2011, 2011. 13141

Liu, X., Penner, J. E., Ghan, S. J., and Wang, M.: Inclusion of ice microphysics in the NCAR community atmospheric model version 3 (CAM3), J. Climate, 20, 4526–4547, doi:10.1175/JCLI4264.1, 2007. 13111

Lohmann, U. and Hoose, C.: Sensitivity studies of different aerosol indirect effects in mixed-phase clouds, Atmos. Chem. Phys., 9, 8917–8934, doi:10.5194/acp-9-8917-2009, 2009. 13111

ACPD
15, 13109–13166, 2015

Lüönd, F., Stetzer, O., Welti, A., and Lohmann, U.: Experimental study on the ice nucleation ability of size-selected kaolinite particles in the immersion mode, J. Geophys. Res., 115, D14201, doi:10.1029/2009JD012959, 2010. 13113, 13116, 13139

Marcolli, C., Gedamke, S., Peter, T., and Zobrist, B.: Efficiency of immersion mode ice nucleation on surrogates of mineral dust, Atmos. Chem. Phys., 7, 5081–5091, doi:10.5194/acp-7-5081-2007, 2007. 13113, 13116, 13122, 13123

McFarquhar, G. M., Zhang, G., Poellot, M. R., Kok, G. L., McCoy, R., Tooman, T., Fridlind, A., and Heymsfield, A. J.: Ice properties of single-layer stratocumulus during the Mixed-Phase Arctic Cloud Experiment: 1. Observations, J. Geophys. Res., 112, D24201, doi:10.1029/2007jd008633, 2007. 13141

Möhler, O., Stetzer, O., Schaefers, S., Linke, C., Schnaiter, M., Tiede, R., Saathoff, H., Krämer, M., Mangold, A., Budz, P., Zink, P., Schreiner, J., Mauersberger, K., Haag, W., Kärcher, B., and Schurath, U.: Experimental investigation of homogeneous freezing of sulphuric acid particles in the aerosol chamber AIDA, Atmos. Chem. Phys., 3, 211–223, doi:10.5194/acp-3-211-2003, 2003. 13138

Murphy, D. M. and Koop, T.: Review of the vapour pressures of ice and supercooled water for atmospheric applications, Q. J. Roy. Meteor. Soc., 131, 1539–1565, doi:10.1256/qj.04.94, 2005. 13118

Murray, B. J., Broadley, S. L., Wilson, T. W., Atkinson, J. D., and Wills, R. H.: Heterogeneous freezing of water droplets containing kaolinite particles, Atmos. Chem. Phys., 11, 4191–4207, doi:10.5194/acp-11-4191-2011, 2011. 13113, 13116, 13118, 13124, 13133

Murray, B. J., O'Sullivan, D., Atkinson, J. D., and Webb, M. E.: Ice nucleation by particles immersed in supercooled cloud droplets, Chem. Soc. Rev., 41, 6519–6554, doi:10.1039/C2CS35200A, 2012. 13131

Myhre, G., Shindell, D., Bréon, F.-M., Collins, W., Fuglestvedt, J., Huang, J., Koch, D., Lamarque, J.-F., Lee, D., Mendoza, B., Nakajima, T., Robock, A., Stephens, G., Takemura, T., and Zhang, H.: Anthropogenic and natural radiative forcing, chapt. 8, in: Climate Change 2013: The Physical Science Basis. Contribution of Working Group I to the Fifth Assessment Report of the Intergovernmental Panel on Climate Change, Cambridge University Press, Cambridge, UK and New York, NY, USA, 659–740, 2013. 13112

Niedermeier, D., Hartmann, S., Shaw, R. A., Covert, D., Mentel, T. F., Schneider, J., Poulain, L., Reitz, P., Spindler, C., Clauss, T., Kiselev, A., Hallbauer, E., Wex, H., Mildenberger, K., and Stratmann, F.: Heterogeneous freezing of droplets with immersed mineral

ACPD
15, 13109–13166, 2015

dust particles – measurements and parameterization, Atmos. Chem. Phys., 10, 3601–3614, doi:10.5194/acp-10-3601-2010, 2010. 13113, 13116
Niedermeier, D., Shaw, R. A., Hartmann, S., Wex, H., Clauss, T., Voigtländer, J., and Stratmann, F.: Heterogeneous ice nucleation: exploring the transition from stochastic to singular freezing behavior, Atmos. Chem. Phys., 11, 8767–8775, doi:10.5194/acp-11-8767-2011, 2011. 13113
Niemand, M., Möhler, O., Vogel, B., Vogel, H., Hoose, C., Connolly, P., Klein, H., Bingemer, H., DeMott, P., Skrotzki, J., and Leisner, T.: A particle-surface-area-based parameterization of immersion freezing on desert dust particles, J. Atmos. Sci., 69, 3077–3092, doi:10.1175/JAS-D-11-0249.1, 2012. 13113, 13114, 13133, 13134, 13135, 13138, 13143, 13156, 13164
O'Sullivan, D., Murray, B. J., Malkin, T. L., Whale, T. F., Umo, N. S., Atkinson, J. D., Price, H. C., Baustian, K. J., Browse, J., and Webb, M. E.: Ice nucleation by fertile soil dusts: relative importance of mineral and biogenic components, Atmos. Chem. Phys., 14, 1853–1867, doi:10.5194/acp-14-1853-2014, 2014. 13138
Park, K., Dutcher, D., Emery, M., Pagels, J., Sakurai, H., Scheckman, J., Qian, S., Stolzenburg, M. R., Wang, X., Yang, J., and McMurry, P. H.: Tandem measurements of aerosol properties-A review of mobility techniques with extensions, Aerosol Sci. Tech., 42, 801–816, doi:10.1080/02786820802339561, 2008. 13114, 13132
Pinti, V., Marcolli, C., Zobrist, B., Hoyle, C. R., and Peter, T.: Ice nucleation efficiency of clay minerals in the immersion mode, Atmos. Chem. Phys., 12, 5859–5878, doi:10.5194/acp-12-5859-2012, 2012. 13113, 13122, 13123, 13133
Prenni, A. J., Demott, P. J., Rogers, D. C., Kreidenweis, S. M., McFarquhar, G. M., Zhang, G., and Poellot, M. R.: Ice nuclei characteristics from M-PACE and their relation to ice formation in clouds, Tellus B, 61, 436–448, 2009. 13141
Pruppacher, H., R. and Klett, J. D.: Microphysics of Clouds and Precipitation, Kluwer Academic Publishers, Dordrecht, Netherlands, 1997. 13111, 13112, 13116
Riechers, B., Wittbracht, F., Hutten, A., and Koop, T.: The homogeneous ice nucleation rate of water droplets produced in a microfluidic device and the role of temperature uncertainty, Phys. Chem. Chem. Phys., 15, 5873–5887, doi:10.1039/C3CP42437E, 2013. 13137
Reddington, C. L., McMeeking, G., Mann, G. W., Coe, H., Frontoso, M. G., Liu, D., Flynn, M., Spracklen, D. V., and Carslaw, K. S.: The mass and number size distributions of black carbon aerosol over Europe, Atmos. Chem. Phys., 13, 4917–4939, doi:10.5194/acp-13-4917-2013, 2013. 13113, 13114, 13116, 13138

ACPD
15, 13109–13166, 2015

Rogers, D. C., DeMott, P. J., Kreidenweis, S. M., and Chen, Y. L.: A continuous-flow diffusion chamber for airborne measurements of ice nuclei, J. Atmos. Ocean. Tech., 18, 725–741, 2001. 13132

Rosenfeld, D., Andreae, M. O., Asmi, A., Chin, M., de Leeuw, G., Donovan, D. P., Kahn, R., Kinne, S., Kivekäs, N., Kulmala, M., Lau, W., Schmidt, K. S., Suni, T., Wagner, T., Wild, M., and Quaas, J.: Global observations of aerosol-cloud-precipitation-climate interactions, Rev. Geophys., 52, 750–808, doi:10.1002/2013RG000441, 2014. 13111

Rossow, W. and Schiffer, R.: Advances in understanding clouds from ISCCP, B. Am. Meteorol. Soc., 80, 2261–2287, doi:10.1175/1520-0477(1999)080<2261:AIUCFI>2.0.CO;2, 1999. 13111

Schill, G. P. and Tolbert, M. A.: Heterogeneous ice nucleation on phase-separated organic-sulfate particles: effect of liquid vs. glassy coatings, Atmos. Chem. Phys., 13, 4681–4695, doi:10.5194/acp-13-4681-2013, 2013. 13138

Schmid, O., Karg, E., Hagen, D. E., Whitefield, P. D., and Ferron, G. A.: On the effective density of non-spherical particles as derived from combined measurements of aerodynamic and mobility equivalent size, J. Aerosol Sci., 38, 431–443, doi:10.1016/j.jaerosci.2007.01.002, 2007. 13114, 13132

Slowik, J. G., Stainken, K., Davidovits, P., Williams, L. R., Jayne, J. T., Kolb, C. E., Worsnop, D. R., Rudich, Y., DeCarlo, P. F., and Jimenez, J. L.: Particle morphology and density characterization by combined mobility and aerodynamic diameter measurements. Part 2: Application to combustion-generated soot aerosols as a function of fuel equivalence ratio, Aerosol Sci. Tech., 38, 1206–1222, doi:10.1080/027868290903916, 2004. 13114, 13132

Stetzer, O., Baschek, B., Luond, F., and Lohmann, U.: The Zurich Ice Nucleation Chamber (ZINC) – a new instrument to investigate atmospheric ice formation, Aerosol Sci. Tech., 42, 64–74, 2008. 13139

Szakáll, M., Diehl, K., Mitra, S. K., and Borrmann, S.: A wind tunnel study on the shape, oscillation, and internal circulation of large raindrops with sizes between 2.5 and 7.5 mm, J. Atmos. Sci., 66, 755–765, doi:10.1175/2008JAS2777.1, 2009. 13138

Tajiri, T., Yamashita, K., Murakami, M., Saito, A., Kusunoki, K., Orikasa, N., and Lilie, L.: A novel adiabatic-expansion-type cloud simulation chamber, J. Meteorol. Soc. Jpn., 91, 687–704, doi:10.2151/jmsj.2013-509, 2013. 13138

Tao, W.-K., Chen, J.-P., Li, Z., Wang, C., and Zhang, C.: Impact of aerosols on convective clouds and precipitation, Rev. Geophys., 50, RG2001, doi:10.1029/2011RG000369, 2012. 13111

ACPD
15, 13109–13166, 2015

Tobo, Y., Prenni, A. J., DeMott, P. J., Huffman, J. A., McCluskey, C. S., Tian, G., Pöhlker, C., Pöschl, U., and Kreidenweis, S. M.: Biological aerosol particles as a key determinant of ice nuclei populations in a forest ecosystem, J. Geophys. Res., 118, 10100–10110, doi:10.1002/jgrd.50801, 2013. 13139

Vali, G.: Quantitative evaluation of experimental results on heterogeneous freezing nucleation of supercooled liquids, J. Atmos. Sci., 29, 402–409, doi:10.1175/1520-0469(1971)028<0402:QEOERA>2.0.CO;2, 1971. 13113

Vali, G.: Repeatability and randomness in heterogeneous freezing nucleation, Atmos. Chem. Phys., 8, 5017–5031, doi:10.5194/acp-8-5017-2008, 2008. 13113

Vali, G. and Snider, J. R.: Time-dependent freezing rate parcel model, Atmos. Chem. Phys., 15, 2071–2079, doi:10.5194/acp-15-2071-2015, 2015. 13113

Welti, A., Lüönd, F., Stetzer, O., and Lohmann, U.: Influence of particle size on the ice nucleating ability of mineral dusts, Atmos. Chem. Phys., 9, 6705–6715, doi:10.5194/acp-9-6705-2009, 2009. 13139

Welti, A., Lüönd, F., Kanji, Z. A., Stetzer, O., and Lohmann, U.: Time dependence of immersion freezing: an experimental study on size selected kaolinite particles, Atmos. Chem. Phys., 12, 9893–9907, doi:10.5194/acp-12-9893-2012, 2012. 13114, 13139

Wex, H., DeMott, P. J., Tobo, Y., Hartmann, S., Rösch, M., Clauss, T., Tomsche, L., Niedermeier, D., and Stratmann, F.: Kaolinite particles as ice nuclei: learning from the use of different kaolinite samples and different coatings, Atmos. Chem. Phys., 14, 5529–5546, doi:10.5194/acp-14-5529-2014, 2014. 13114, 13131, 13132, 13133, 13136, 13139, 13143, 13163

Wright, T. P. and Petters, M. D.: The role of time in heterogeneous freezing nucleation, J. Geophys. Res., 118, 3731–3743, doi:10.1002/jgrd.50365, 2013. 13114, 13117, 13121, 13122, 13123, 13138, 13143, 13157

Zelenyuk, A., Cai, Y., and Imre, D.: From agglomerates of spheres to irregularly shaped particles: determination of dynamic shape factors from measurements of mobility and vacuum aerodynamic diameters, Aerosol Sci. Tech., 40, 197–217, doi:10.1080/02786820500529406, 2006. 13114, 13132

Zobrist, B., Koop, T., Luo, B. P., Marcolli, C., and Peter, T.: Heterogeneous ice nucleation rate coefficient of water droplets coated by a nonadecanol monolayer, J. Phys. Chem. A, 111, 2149–2155, doi:10.1021/jp066080w, 2007. 13112, 13113

ACPD
15, 13109–13166, 2015

Zuberi, B., Bertram, A., Cassa, C. A., Molina, L. T., and Molina, M. J.: Heterogeneous nucleation of ice in $(NH_4)_2SO_4$-H_2O particles with mineral dust immersions, Geophys. Res. Lett., 29, 1504, doi:10.1029/2001GL014289, 2002. 13114

ACPD
15, 13109–13166, 2015

Table 1. Summary of parameters used in isothermal model simulations.

Name	N_{tot}	σ_g	A_g / cm^2	T / K	J_{het} cm^{-2} s^{-1}	IN Type	Figure	Color
Iso1	1000	1	1.0×10^{-5}	–	1.0×10^{3}	–	1a	dark green
Iso2	30	1	1.0×10^{-5}	–	1.0×10^{3}	–	1a	light green
Iso3	1000	10	1.0×10^{-5}	–	1.0×10^{3}	–	1a	dark blue
Iso4	30	10	1.0×10^{-5}	–	1.0×10^{3}	–	1a	light blue
IsoWR	1000	9.5	6.4×10^{-3}	251.15	6.0×10^{-4}	ATD[a]	1b	orange
IsoBR	63	8.3	2.6×10^{-7}	243.3	1.3×10^{3}	illite	2a	orange
IsoHE1	40	2.2	1.2×10^{0}	255.15	4.1×10^{-3}	kaolinite	2b	orange
IsoHE2	40	8.5	2.0×10^{-2}	262.15	2.0×10^{-2}	feldspar	2c	orange
IsoDI1	45	4.2	5.1×10^{-1}	255.15	1.3×10^{-2}	illite	3	green
IsoDI2	45	9.1	5.1×10^{-2}	252.15	9.5×10^{-1}	illite	3	orange
IsoDI3	45	1.5	5.1×10^{-1}	252.15	8.3×10^{-1}	illite	3	blue
IsoCFDC	833	7.7	6.2×10^{-8}	238.65–247.65[b]	ABIFM[c]	kaolinite	7	blue, green
IsoLACIS	21	7.7	6.2×10^{-8}	235.65–238.65[b]	ABIFM[c]	kaolinite	7	orange, black

[a] Arizona Test Dust.
[b] Isothermal simulations were performed at 0.15 K increments within the stated temperature range.
[c] Values of J_{het} are calculated from the water activity, a_w, based immersion freezing model (ABIFM) (Knopf and Alpert, 2013).

ACPD
15, 13109–13166, 2015

Table 2. Summary of parameters used in cooling rate model simulations.

Name	N_{tot}	σ_g	A_g / cm^2	m	c	r / K min^{-1}	IN Type	Figure	Color
Cr1	1000	10	1.0×10^{-5}	54.48	−10.67	0.5	illite	4	orange
Cr2	1000	10	1.0×10^{-5}	54.48	−10.67	5.0	illite	4	blue
CrHE1	40	8.5	2.1×10^{-2}	122.83	−12.98	0.2	feldspar	5	orange
CrHE2	40	8.5	2.1×10^{-2}	122.83	−12.98	2.0	feldspar	5	blue
CrDI1	45	5.7	2.9×10^{0}	54.48	−10.67	non-linear[a]	illite	6	orange
CrDI2	45	5.7	2.9×10^{-2}	54.48	−10.67	non-linear[a]	illite	6	blue
	A_{tot} / cm^2		$D_{p,g}$ / µm						
CrNI1	6.5×10^{-4}	1.72	0.42	22.91	−1.27	non-linear[b]	ND[c]	8	blue
CrNI2	5.4×10^{-4}	1.69	0.40	22.91	−1.27	non-linear[b]	ND[c]	8	orange
	N_{tot}								
MPC1	10^7	1	0.3	54.48	−10.67	0.36	illite	10	red
MPC2	10^7	5	0.3	54.48	−10.67	0.36	illite	10	blue

[a] A continuous non-linear cooling rate with time is given in Diehl et al. (2014).
[b] A continuous non-linear cooling rate with time due to adiabatic expansion is fitted to experimental trajectories (Niemand et al., 2012) using a 4th order polynomial.
[c] Natural dusts from Niemand et al. (2012): Asian, Saharan, Israeli and Canary Island dust.

ACPD
15, 13109–13166, 2015

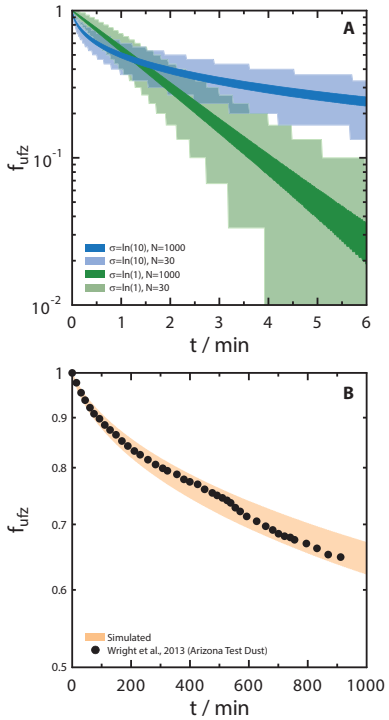

Figure 1. Sensitivity calculations of the unfrozen droplet fraction, f_{ufz}, as a function time, t, derived from model simulations for a total number of droplets, N_{tot}, and variability of ice nuclei surface area, σ_g. **(a)** Model simulated 5 and 95 % bounds of f_{ufz} are shown as dark green (Iso1), light green (Iso2), dark blue (Iso3), and light blue (Iso4) shading. Parameter values are given in the legend. **(b)** Simulated 5 and 95 % bounds of f_{ufz} derived from IsoWR are shown as the orange shading along with experimental data of isothermal immersion freezing by Arizona test dust (Wright and Petters, 2013) shown as black circles. Parameter values for all model simulations in **(a)** and **(b)** are given in Table 1.

ACPD
15, 13109–13166, 2015

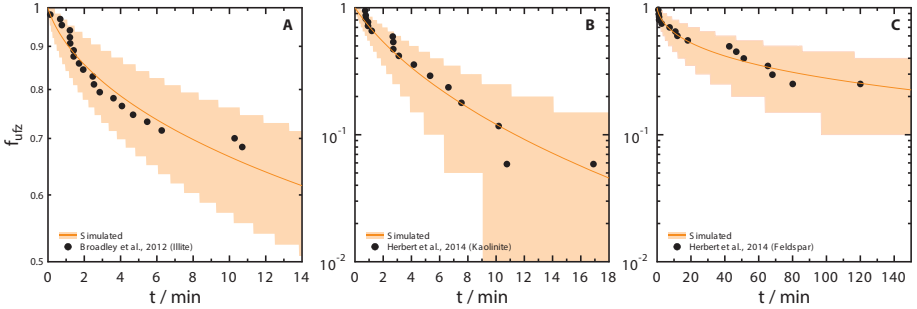

Figure 2. Simulated and experimentally (Broadley et al., 2012; Herbert et al., 2014) derived unfrozen droplet fractions, f_{ufz}, as a function time, t. Model simulations and IN types used are: **(a)** IsoBR and illite, **(b)** IsoHE1 and kaolinite, and **(c)** IsoHE2 and feldspar, respectively. Orange lines and shading represent $\bar{f}_{ufz}$ and corresponding 5 and 95 % bounds, respectively. Parameter values for model simulations are given in Table 1.

ACPD
15, 13109–13166, 2015

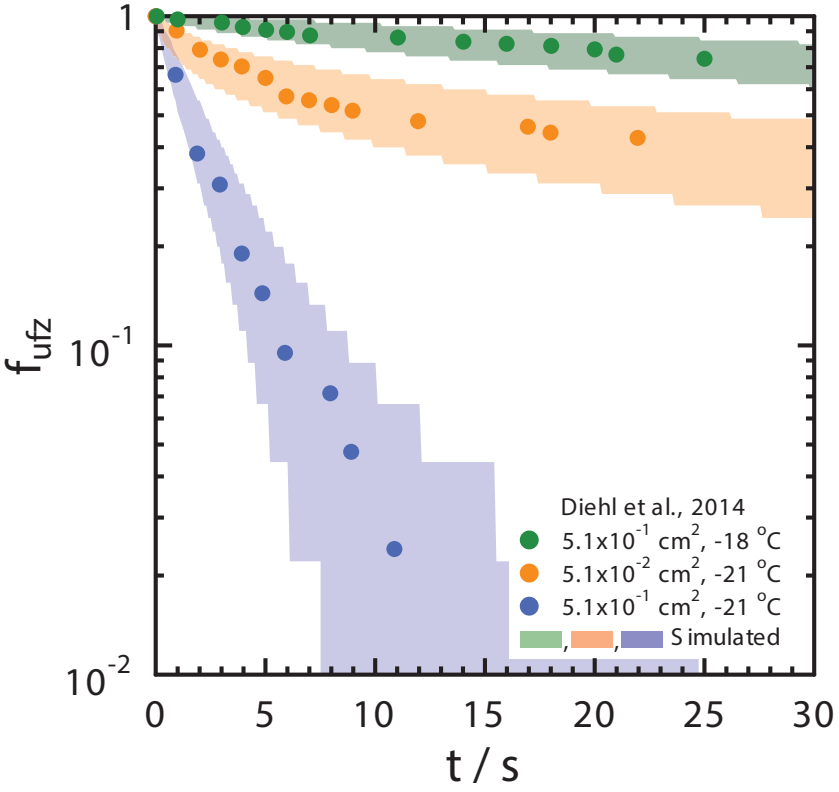

Figure 3. Simulated and experimentally (Diehl et al., 2014) derived unfrozen droplet fractions, f_{ufz}, as a function time, t, using illite. Model simulated 5 and 95% bounds of f_{ufz} are shown as green, orange and blue shading for IsoDI1, IsoDI2 and IsoDI3, respectively. Temperature and average surface area per droplet reported by Diehl et al. (2014) are given in the legend. Parameter values for model simulations are given in Table 1.

ACPD
15, 13109–13166, 2015

A unifying ice nucleation model

P. A. Alpert and
D. A. Knopf

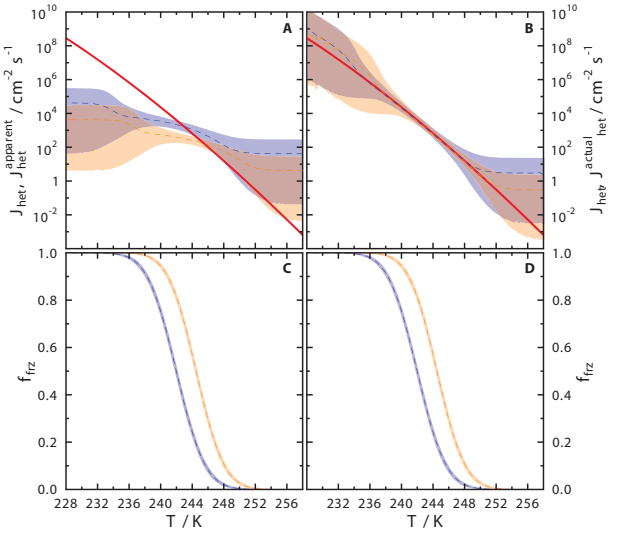

Figure 4. Sensitivity calculations of heterogeneous ice nucleation rate coefficients, J_{het}, and frozen droplet fractions, f_{frz}, on cooling rate, r, derived from model simulations Cr1 (orange) and Cr2 (blue) where r = 0.5 and 5.0 K min^{-1}, respectively. J_{het} as a function of temperature, T, are shown in **(a)** assuming uniform ice nuclei surface area (ISA) per droplet yielding $J_{het}^{apparent}$, and (B) accounting for different ISA yielding J_{het}^{actual}. The dashed lines in **(a)** and **(b)** are $\overline{J}_{het}^{apparent}$ and $\overline{J}_{het}^{actual}$, respectively. Shadings in **(a)** and **(b)** correspond to upper and lower fiducial limits with x = 0.999 confidence and the solid red line is calculated from Eq. (4) for illite (Knopf and Alpert, 2013). Frozen droplet fractions, f_{frz}, are shown in **(c)** and **(d)** where dashed lines and shadings represent $\overline{f}_{frz}$ and 5 and 95 % bounds, respectively. Parameter values for Cr1 and Cr2 are given in Table 2.

ACPD
15, 13109–13166, 2015

A unifying ice nucleation model

P. A. Alpert and
D. A. Knopf

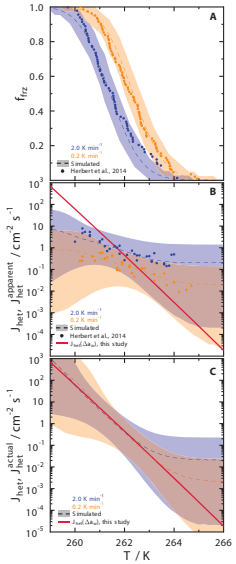

Figure 5. Frozen droplet fractions, f_{frz}, and heterogeneous ice nucleation rate coefficients, J_{het}, from immersion freezing cooling rate, r, dependent model simulations CrHE1 and CrHE2 where r = 0.2 (orange) and 2.0 K min^{-1} (blue), respectively, and experimental data of feldspar acting as immersion IN (Herbert et al., 2014). Dashed lines and shadings in **(a)** are $\overline{f}_{frz}$ and 5 and 95 % bounds, respectively. J_{het} as a function of temperature, T, are shown in **(b)** assuming uniform ice nuclei surface area (ISA) per droplet yielding $J_{het}^{apparent}$ and **(c)** accounting for variable ISA yielding J_{het}^{actual}. The dashed lines in **(b)** and **(c)** are $\overline{J}_{het}^{apparent}$ and $\overline{J}_{het}^{actual}$, respectively. Shadings in **(b)** and **(c)** correspond to upper and lower fiducial limits with x = 0.999 confidence. Experimentally derived f_{frz} and J_{het} are shown as circles in **(a)** and **(b)**, respectively (Herbert et al., 2014). The red line in **(b)** and **(c)** is calculated from Eq. (4) (Knopf and Alpert, 2013) using new parameters derived for feldspar. Parameter values for CrHE1 and CrHE2 are given in Table 2.

ACPD
15, 13109–13166, 2015

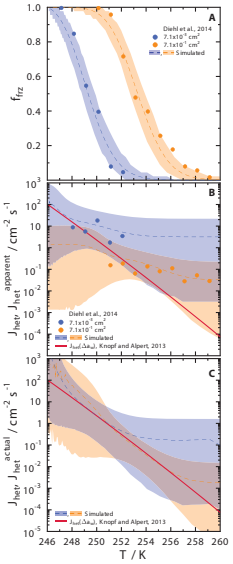

Figure 6. Frozen droplet fractions, f_{frz}, and heterogeneous ice nucleation rate coefficients, J_{het}, from immersion freezing model simulations CrDI1 (orange) and CrDI2 (blue), and experimental data of illite acting as immersion IN are shown (Diehl et al., 2014). Dashed lines and shadings in **(a)** are $\bar{f}_{frz}$ and 5 and 95 % bounds, respectively. J_{het} as a function of temperature, T, are shown in **(b)** assuming uniform ice nucleating particle surface area (ISA) per droplet yielding $J_{het}^{apparent}$ and **(c)** accounting for variable ISA yielding J_{het}^{actual}. The dashed lines in **(b)** and **(c)** are $\bar{J}_{het}^{apparent}$ and $\bar{J}_{het}^{actual}$, respectively. Shadings in **(b)** and **(c)** correspond to upper and lower fiducial limits with $x = 0.999$ confidence. Experimentally derived f_{frz} and J_{het} are shown as circles in **(a)** and **(b)**, respectively (Diehl et al., 2014). The red line in **(b)** and **(c)** is calculated from Eq. (4) for illite (Knopf and Alpert, 2013). Parameter values for CrDI1 and CrDI2 are given in Table 2.

ACPD
15, 13109–13166, 2015

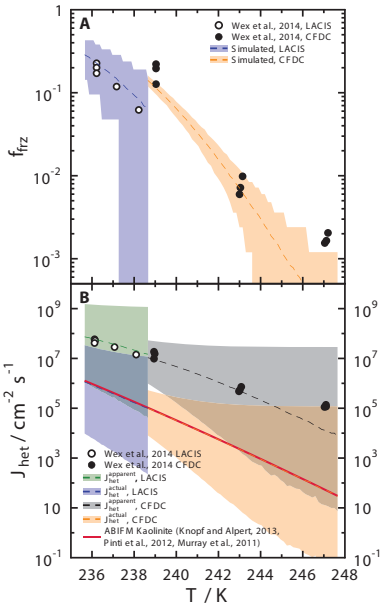

Figure 7. Frozen droplet fractions, f_{frz}, and heterogeneous ice nucleation rate coefficients, J_{het}, from isothermal model simulations IsoCFDC (orange and black) and IsoLACIS (blue and green), and experimental data of immersion freezing due to kaolinite by Wex et al. (2014) are shown. Dashed lines and shadings in **(a)** are $\bar{f}_{frz}$ and 5 and 95 % bounds, respectively. J_{het} as a function of temperature, T, are shown in **(b)** assuming uniform ice nucleating particle surface area (ISA) per droplet yielding $J_{het}^{apparent}$, and accounting for variable ISA yielding J_{het}^{actual}. The dashed lines in **(b)** are $\bar{J}_{het}^{apparent}$ and $\bar{J}_{het}^{actual}$ as indicated in the legend. Shadings in **(b)** correspond to upper and lower fiducial limits with $x = 0.999$ confidence and the red line is calculated from Eq. (4) for kaolinite (Knopf and Alpert, 2013). Parameter values for IsoCFDC and IsoLACIS are given in Table 1.

ACPD
15, 13109–13166, 2015

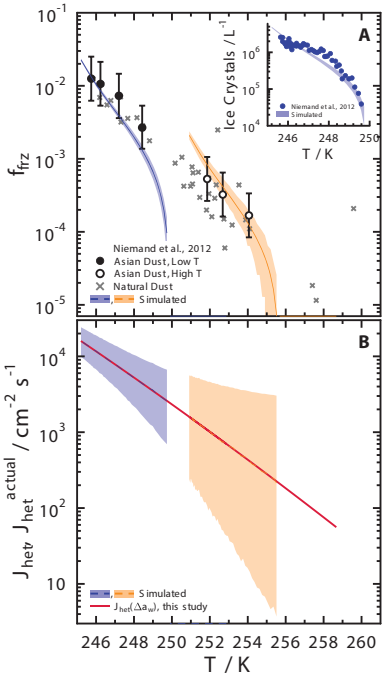

Figure 8. Frozen droplet fractions, f_{frz}, and heterogeneous ice nucleation rate coefficients, J_{het}, derived from adiabatic cooling immersion freezing model simulations CrNI1 (blue) and CrNI2 (orange). Simulated and experimentally observed ice crystal concentrations are shown in the insert of panel **(a)**. Dashed lines and shadings in **(a)** are $\bar{f}_{frz}$ and 5 and 95 % bounds, respectively. Experimentally derived f_{frz} and uncertainties by Niemand et al. (2012) are shown as symbols and error bars. J_{het} as a function of temperature, T, is shown in **(b)** and accounting for variable ISA yielding J_{het}^{actual}, where dashed lines and shading are $\bar{J}_{het}^{actual}$ and fiducial limits with $x = 0.999$ confidence, respectively. The red line in **(b)** is calculated from Eq. (4) using new parameters derived for natural dust. Parameter values for CrNI1 and CrNI2 are given in Table 2.

ACPD
15, 13109–13166, 2015

A unifying ice nucleation model

P. A. Alpert and D. A. Knopf

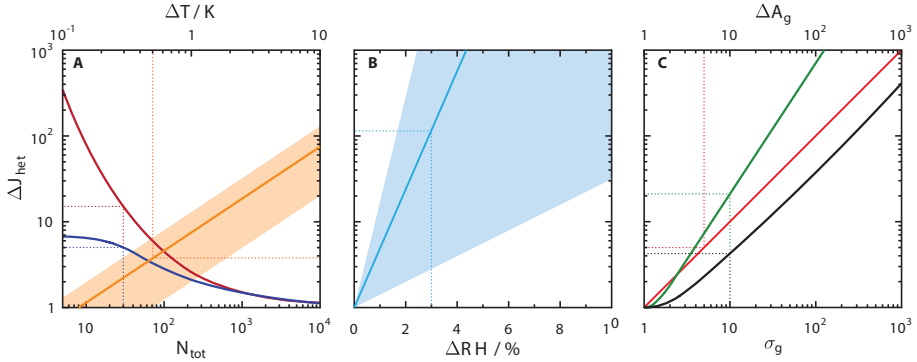

Figure 9. Uncertainty analysis derived from immersion freezing model simulations. The relative error in the experimentally derived heterogeneous ice nucleation rate coefficient, J_{het}, is referred to as ΔJ_{het}. The y axis indicates ΔJ_{het} as a factor error, e.g. $\Delta J_{het} = 10$ indicates an error in J_{het} by a factor of 10 in the positive and negative direction. Statistical error due to the applied number of droplets, N_{tot}, is shown in **(a)** where red and blue represent the upper and lower fiducial limits of J_{het}, respectively. The error due to temperature accuracy, ΔT, for a variety of IN types is shown in **(a)** in orange color where the solid line is average ΔJ_{het} as a function of ΔT and the shading is for a range of IN types. The error due to the absolute uncertainty in water activity or equivalently relative humidity, ΔRH, is shown in **(b)** where the blue line is average ΔJ_{het}, and the shading represents the range of values for a variety of IN types. The uncertainty due to variability in IN surface area, σ_g, is shown in **(c)** as black and green lines evaluated at $f_{frz} = 0.1$ and 0.9, respectively. The uncertainty in measuring absolute surface area, ΔA_g, is shown in **(c)** as the red line. Further details and example uncertainty values given as dotted lines are described in the text.

ACPD
15, 13109–13166, 2015

A unifying ice nucleation model

P. A. Alpert and
D. A. Knopf

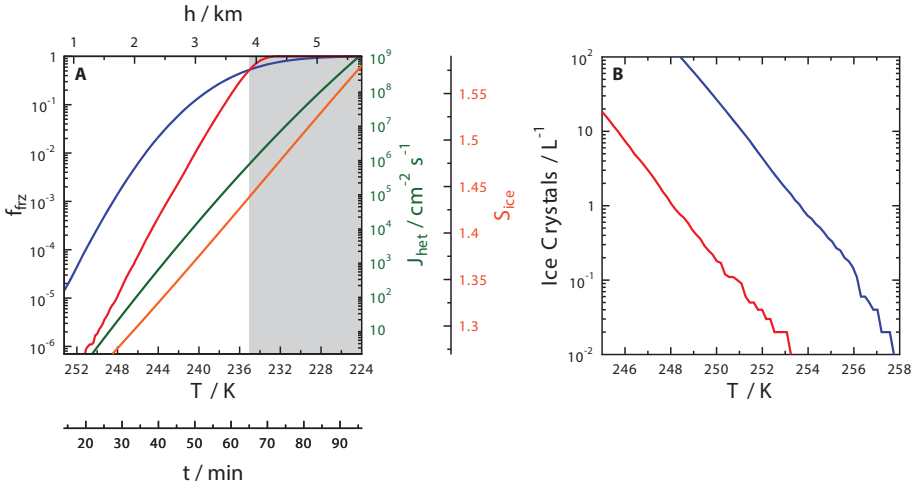

Figure 10. Results of two ice nucleation models for mixed-phase cloud conditions (MPC1 and MPC2) considering uniform ($\sigma_g = 1$) or lognormally ($\sigma_g = 5$) distributed IN diameters, D_p, respectively. Median D_p for both is 300 nm. Parameter values for MPC1 and MPC2 are given in Table 2. Immersion freezing is simulated for 10^7 particles in 100 L of air with an updraft velocity, $w = 100\,\mathrm{cm\,s^{-1}}$ and a lapse rate, $\Gamma = 6\,\mathrm{K\,km^{-1}}$. Frozen droplet fraction, f_{frz}, is shown in **(a)** as a function of temperature, T, time, t, and height, h, for MPC1 and MPC2 as red and blue lines, respectively. The green line is the heterogeneous ice nucleation rate coefficient, J_{het}, calculated using Eq. (4) for illite (Knopf and Alpert, 2013) and the orange line is the ice saturation ratio, S_{ice}. **(b)** Ice crystals per liter of air derived from MPC1 and MPC2 are given by the red and blue lines, respectively.

ACPD
15, 13109–13166, 2015

A unifying ice nucleation model

P. A. Alpert and D. A. Knopf